Contributions to Mineralogy and Petrology (2022) 177:54
https://doi.org/10.1007/s00410-022-01918-5

ORIGINAL PAPER

Garnet EoS: a critical review and synthesis

Ross J. Angel[1] · **Mattia Gilio**[2] · **Mattia Mazzucchelli**[3] · **Matteo Alvaro**[2]

Received: 20 December 2021 / Accepted: 15 April 2022 / Published online: 6 May 2022

Abstract
All available volume and elasticity data for the garnet end-members grossular, pyrope, almandine and spessartine have been re-evaluated for both internal consistency and for consistency with experimentally measured heat capacities. The consistent data were then used to determine the parameters of third-order Birch–Murnaghan EoS to describe the isothermal compression at 298 K and a Mie–Grüneisen–Debye thermal-pressure EoS to describe the PVT behaviour. In a full Mie–Grüneisen–Debye EoS, the variation of the thermal Grüneisen parameter with volume is defined as $\gamma = \gamma_0\left(\frac{V}{V_0}\right)^q$. For grossular and pyrope garnets, there is sufficient data to refine q which has a value of $q = 0.8(2)$ for both garnets. For other garnets, the data do not constrain the value of q and we therefore refined a q-compromise version of the Mie–Grüneisen–Debye EoS in which both γ/V and the Debye temperature θ_D are held constant at all P and T, leading to $\left(\partial C_V/\partial P\right)_T = 0$, parallel isochors and constant isothermal bulk modulus along an isochor. Final refined parameters for the q-compromise Mie–Grüneisen–Debye EoS are:

	Pyrope	Almandine	Spessartine	Grossular
V_0 (cm^3/mol)[a]	113.13	115.25	117.92	125.35
K_{0T} (GPa)	169.3 (3)	174.6 (4)	177.57 (6)	167.0 (2)
K'_{0T}	4.55 (5)	5.41 (13)	4.6 (3)	5.07 (8)
θ_{D0}	771 (28)	862 (22)	860 (35)	750 (13)
γ_0	1.185 (12)	1.16 (fixed)	1.18 (3)	1.156 (6)

for pyrope and grossular, the two versions of the Mie–Grüneisen–Debye EoS predict indistinguishable properties over the metamorphic pressure and temperature range, and the same properties as the EoS based on experimental heat capacities. The biggest change from previously published EoS is for almandine for which the new EoS predicts geologically reasonable entrapment conditions for zircon inclusions in almandine-rich garnets.

Keywords Garnet equations of state · Pyrope · Grossular · Almandine · Spessartine

Communicated by Timothy L. Grove.

✉ Ross J. Angel
ross.angel@igg.cnr.it

Mattia Gilio
mattia.gilio@unipv.it

Mattia Mazzucchelli
mmazzucc@uni-mainz.de

Matteo Alvaro
matteo.alvaro@unipv.it

[1] IGG CNR, Via Giovanni Gradenigo 6, 35131 Padova, Italy

[2] Department of Earth and Environmental Sciences, University of Pavia, Via A. Ferrata 1, 27100 Pavia, Italy

[3] Mainz Institute of Multiscale Modelling and Institute of Geosciences, Johannes-Gutenberg University of Mainz, J.-J.-Becher-Weg 21, 55128 Mainz, Germany

Introduction

Garnets are vitally important in metamorphic petrology, especially because they trap and preserve high-pressure and high-temperature phases which are quite often the other products of the garnet-forming reaction. Accurate Equations of State (EoS) to describe the volume variations of garnet with P and T are therefore required to calculate phase equilibria that indicate the conditions under which the garnets grew and trapped their inclusions. EoS are also required to interpret the remanent pressures, stresses and strains in inclusion phases to recalculate the entrapment conditions by the rapidly developing methods of elastic geobarometry (e.g. Zhong et al. 2018, 2020; Alvaro et al. 2020; Morganti et al. 2020; Mazzucchelli et al. 2021). However, the large differences in published EoS even for the end-member garnets pyrope, grossular, almandine and spessartine often prevent meaningful or reliable geological information to be obtained from the stress states of inclusions trapped within them.

EoS of garnets, as for all minerals, comprise two components. One is the equation or equations that relate volume to pressure and temperature under hydrostatic pressure. The EoS therefore also defines the isothermal Reuss bulk modulus as the pressure derivative of the volume which is $K_T = -V(\partial P/\partial V)_T$, and other derivatives such as $K'_T = \left(\partial K_T/\partial P\right)_T$, the thermal expansion coefficient $\alpha = \frac{1}{V}(\partial V/\partial T)_P$, and the variation of bulk modulus with temperature $\left(\partial K_T/\partial T\right)_P$. The second component of an EoS for a specific mineral is the set of values for the parameters that appear in the equations. These parameters are denoted with a subscript 0, indicating the parameter value at the reference T and P conditions, usually taken as room conditions ($T \sim 298$ K, 25 °C and $P \sim 1$ bar). Thus, K_{T0} is the isothermal Reuss bulk modulus at the reference conditions. The parameter sets are not the same for all types of EoS. For example, while α_0, the volume thermal expansion coefficient at reference conditions, is a parameter of some isothermal EoS, it does not appear explicitly in the Mie–Grüneisen–Debye EoS although the thermal expansion coefficient at room conditions can be calculated from it. Once an equation for an EoS has been chosen, the parameter values are determined by least-squares refinement to experimental data for volumes or bulk moduli measured over a range of P and T.

Despite the challenges of performing accurate and precise measurements of elastic properties of minerals at high P and T, there is an ever-increasing amount of new internally consistent and precise data for garnets, especially measurements of their bulk moduli at simultaneous high P and T. However, these data are often fitted on their own to obtain EoS parameters that are then compared, in often very extensive tables, to the results of fitting data from other experimental studies. Such independent fits of individual datasets inevitably suffer from large uncertainties in the parameter values, because of the small numbers of data points. And the correlations between the values of parameters are almost never reported or considered, although these are critical for evaluating whether one set of parameters is statistically the same as, or significantly different from, another set of parameters (Angel 2000; Diella et al. 2004; Gréaux and Yamada 2014). Direct experimental measurements of elastic properties yield moduli that are adiabatic, not the isothermal values required for calculating P–V–T relationships. The adiabatic bulk modulus is $K_S = (1 + \alpha\gamma T)K_T$ in which γ is the thermal Grünesien parameter. Since both α and γ are themselves properties of the EOS and therefore vary with P and T, the elastic moduli data alone do not define the volume variation of the mineral, and fits to elastic data alone have to use independent determinations of α and γ as well as $\left(\partial K_T/\partial T\right)_P$ to obtain a PVT relationship (e.g. Kono et al. 2010; Zou et al. 2012b; Gwanmesia et al. 2014).

Further, fitting individual datasets and comparing parameter values do not allow the consistency of individual data to be tested. Individual outliers within datasets, which can be influential in determining the values of the EoS parameters, cannot be identified by comparing the parameter values obtained by fitting different datasets. Neither does fitting individual datasets allow the leverage of different types of data to be exploited; as noted, elastic moduli data do not determine volumes. Similarly, determining elastic moduli from measured volume variations with pressure is challenging and subject to relatively large uncertainties because the moduli are the derivatives of the P–V data values, not the measured data themselves. Consequently, fitting of individual datasets does not allow the values of all of the EoS parameters to be reliably and independently determined, and often forces results to be analysed with over-simplified and over-constrained EoS which in turn can lead to biased parameter values.

Therefore, in this paper, we use end-member garnets as an example to demonstrate how to determine the EoS of minerals from all of the available data for volume, density, and elasticity, using the fitting methods originally developed for analyses of the EoS of grossular garnet (Milani et al. 2017) and mantle olivine (Angel et al. 2018). In addition to these methods, we introduce the use of heat capacity data to identify individual and sets of volume and elasticity data that are in error, for example, errors in their pressure scales or temperature calibrations, or systematic offsets in their data values. Dataset scaling (Ehlers et al. 2022) then allows some of these datasets to be used to constrain the EoS parameters.

In the next section, we describe the types of data available to constrain the EoS of garnets, and how each type of

data can be incorporated into a fit of a single EoS or, as in the case of heat capacity data, used as external validation tool or constraint for the EoS. We discuss the advantages of using the Mie–Grünesien–Debye (MGD) EoS compared to other EoS that have been used to describe the variation of volume and elasticity of garnets with P and T and show why it is physically more realistic and thermodynamically consistent while having less parameters than some alternative approaches. The practical application of these methods is then demonstrated in the following sections in which we describe the analysis of data for each of the major end-member garnets in turn and compare the predicted properties of the new EoS with those of previously published EoS. We describe the implications of this self-consistent set of garnet EoS for elastic geobarometry of other phases included as inclusions in garnets. The EoS are provided in the supplementary material as .eos files that can be used in the EosFit suite of programs (Angel et al. 2014, 2017b; Gonzalez-Platas et al. 2016) which are available as freeware at www.rossangel.net along with the same .eos files for the garnets. The EoS will also be made available for elastic barometry calculations in the EntraPT web application available at www.mineralogylab.com.

Methodology

In this section, we describe the general procedures that we used to process experimental data, and leave the detailed discussion of individual datasets to the sections below on individual garnet end-members, in which we illustrate how we apply these methods in detail.

Data sources

There are three main types of experimental data that can be used to constrain the EoS of garnets; volume and bulk moduli values that may have been determined over a wide range of P and/or T, and heat capacity data determined at room pressure or under vacuum over a range of temperature. Most data are taken from synthetic samples of nominal end-member composition, and near end-member natural samples; exceptions are explicitly noted in the text and tables. Near-end member compositions are expected to have similar volumes and elastic properties to the end-member composition itself (e.g. Newton and Wood 1980), a phenomenon now established as the plateau effect (Salje 1995).

We have scaled various diffraction datasets in various ways to address several sources of inconsistency between datasets. The volumes reported in different published studies are commonly not exactly on the same scale. This can easily be seen if two studies measured their samples at the same P and T but report slightly different V, for example, at room conditions. As a consequence, one could find pairs of datasets in which the first (low) pressure point of one dataset has a larger volume than the ambient pressure datum of second dataset, which without scaling would lead to a non-physical negative value of the bulk modulus. These differences arise from different calibrations of different instruments and not from fitting or measurement uncertainties; for example, various commercial software packages on laboratory X-ray diffractometers use slightly different numerical values for the X-ray wavelengths and so give different volumes for the same material measured at the same conditions. All of the measurements of volume in one diffraction dataset can be expected to be affected equally by these factors. Therefore, if a dataset includes a measurement at room conditions, we scale all of the dataset to that measurement by calculating V/V_0 and then multiply the ratio by the molar volume V_m at the reference conditions. This rescaling does not affect the EoS parameters that are obtained from fitting the individual datasets because all EoS are written in terms of V/V_0, and thus the bulk modulus and its pressure derivatives are independent of the volume scale, but the rescaling is essential to allow simultaneous fitting of multiple datasets. The alternative of refining scale factors to every volume dataset introduces so many additional variables into the refinement that it often becomes unstable. Molar volumes at room conditions were taken from the self-consistent database of Holland and Powell (2011).

Some diffraction datasets, as discussed in detail in the examples, do not include a measurement at the reference conditions by which the data can be scaled. This is often the case for datasets of volumes collected at simultaneous high P and T for which it is difficult or impossible to measure the sample in the same pressure device and diffractometer at room conditions. Therefore, we cannot pre-scale these data to the molar volume at ambient conditions, so we refine a scale factor for these datasets during the least-squares refinement of the EoS parameters (Ehlers et al. 2022). This approach is based on the reasonable assumption that the scaling arises from instrument calibration which remains constant during a series of diffraction measurements. Scale factors are only used for least-squares refinement and are used to multiply the values of V calculated from the EoS to put them on the scale of the measured data. Thus, a scale factor larger than 1.0 indicates that the measured values of the data are larger than those predicted by the EoS. When the scale factor for a group of data refined to 1.0 within the estimated uncertainties, it was reset to 1.0 and not refined further.

Measurements of the adiabatic bulk modulus K_S are often made on polycrystalline samples (e.g. Isaak et al. 1992; Zou et al. 2012b; Gwanmesia et al. 2014; Arimoto et al. 2015; Chantel et al. 2016). Garnets are cubic, so the Reuss and Voigt bounds on the bulk moduli of randomly oriented

polycrystalline samples are identical, and no further scaling should be required to match the K_S determined from the EoS. If scaling is found to be necessary, then it indicates the presence of systematic errors in the data. We have not scaled the K_S values prior to fitting but we have refined scale factors for high-pressure datasets of the bulk moduli that do not yield an extrapolated value of K_{S0} at room conditions in agreement with other datasets or their own measurement (e.g. Arimoto et al. 2015). Use of a constant scale factor assumes that the inconsistencies lie in the values of the moduli and are due to systematic (i.e. constant) errors. This is probably not correct for determinations of bulk moduli by ultrasonic methods which rely also on the determination of sample lengths, and all high P (and P–T) elastic measurements also rely on the pressure calibration. Nonetheless, refinement of a constant scale factor for the bulk moduli is the simplest way by which to achieve consistency between datasets. As for the scale factors applied to volumes, factors are only used for least-squares refinement and are used to multiply the values of K_S calculated from the EoS to put them on the scale of the measured data. Refined scale factors that were 1.0 within the estimated uncertainties were fixed at 1.0 and not refined further.

In addition to scaling the volumes to the molar volumes at room conditions, the last type of rescaling was applied to two PV datasets (Milani et al. 2015, 2017). Their pressures were determined by measuring the unit-cell volume of a quartz crystal mounted in the pressure cell along with the sample crystal. The original EoS for quartz (Angel et al. 1997) used to determine the pressures has been superseded by a new EoS (Scheidl et al. 2016), with which the pressures were recalculated prior to the data being used in the current analysis. This correction to the pressure values results in higher values of the bulk modulus and lower values of K'_T than the published EoS parameters (Milani et al. 2015, 2017), more consistent with direct elasticity measurements.

Some measurements in presses were performed under non-hydrostatic or 'quasi-hydrostatic' conditions because the pressure medium was a solid. Such stress conditions can be characterised by the mean normal stress together with the deviatoric stress field (the difference of the normal stresses from their average). Cubic crystals have the special elastic property that the volume does not depend on the magnitude of the deviatoric stresses, but only on the mean of the normal stresses. Thus the volume of a garnet is always the same as the volume under a hydrostatic pressure equal to the mean normal stress of the non-hydrostatic stress field, provided that there is no plastic deformation of the sample. Therefore, volume data of garnets from non-hydrostatic experiments can also be used to refine the parameters of the hydrostatic EoS, provided that the method of pressure measurement gives the mean normal stress. Experiments in which the pressure was determined from the measured cell volume of a cubic pressure standard (e.g. NaCl or gold) can meet this condition. Pressures determined from diffraction measurements of non-cubic reference crystals such as quartz, or from ruby fluorescence do not yield the mean stress in a non-hydrostatic experiment (e.g. Chai and Brown 1996), and were therefore excluded from our analyses. This is not an issue for diamond-anvil cell measurements in which the pressure medium remained fluid or sufficiently soft that it remains effectively hydrostatic, for example, as in the studies of Milani et al. (2015) and Milani et al. (2017) and the data collected in helium by Zhang et al. (1998).

Equations of state

All thermal (i.e. P–V–T) EoS require that the PV behaviour at room temperature is represented by a conventional EoS. We exclusively use the Birch–Murnaghan (BM EoS), although identical results will be obtained if alternative EoS such as the Tait or Vinet are used. All experimental measurements of the PV compression curves of garnets and their bulk moduli at high pressures show that K'_{T0} is significantly greater than 4, and therefore a third-order BM EoS is required to fit the data. There is no evidence in currently available experimental data that would justify the use of fourth-order EoS.

In the simplest model, widely adopted for analysing elasticity and volume data for garnets, the volume variation at high T and P is then described by isothermal compression at high temperature, and therefore requires the values of V and K_T and K'_T at high temperature and ambient pressure. These are usually provided by assuming that both the thermal expansion coefficient α and $\left(\partial K_T/\partial T\right)_P$ are constants (e.g. Zou et al. 2012b; Fan et al. 2015). A widely used variant is to make the thermal expansion coefficient linear in temperature, as $\alpha = a + bT$ (Gréaux and Yamada 2014, 2019; Arimoto et al. 2015) or a higher order polynomial (Du et al. 2015). While these approaches may be useful in interpolating the values of the EoS parameters within the P and T range of the measured data they should not be used in extrapolation because they are thermodynamically incorrect. In particular, they violate the requirement that both α and $\left(\partial K_T/\partial T\right)_P$ should tend to zero as absolute zero in temperature is approached. Low-temperature data cannot therefore be used to constrain the EoS parameters of these models, and the α and $\left(\partial K_T/\partial T\right)_P$ parameters become the averages over the T range for which data exist and therefore typically over-estimate the value of both parameters at room temperature. Further, the explicit but often unstated assumption that $\left(\partial K'_T/\partial T\right)_P = 0$ will always lead to the EoS exhibiting negative thermal expansion at high pressures (Hellfrich and Connolly 2009) which is not actually observed in garnets.

We therefore use thermal-pressure EoS to overcome these difficulties because they have a basis in the physics

of solids. The compression at room temperature of the garnet to its final volume is still described by a BM3 isothermal EoS which contributes what we denote as P_{ref}, the pressure required at room temperature T_0 to attain the final volume of the garnet. The total pressure at any V and T is the sum of this pressure plus the increase in pressure, ΔPth, on moving along an isochor from the reference temperature to the final temperature:

$$P(V,T) = P_{\mathrm{ref}}\left(V,T_0\right) + \Delta Pth(V,T) \tag{1}$$

The slope of an isochor in P–T space is given by the product $\alpha K_T = \gamma C_{\mathrm{V}}/V_{\mathrm{m}}$, in which γ is the thermal Grüneisen parameter and C_{V} is the isochoric heat capacity per mole, with V_{m} the molar volume. The increase in thermal pressure is thus given by either integral:

$$\Delta Pth = \int_{T0}^{T} \left(\alpha K_{\mathrm{T}}\right)_{\mathrm{V}} \partial T = \int_{T0}^{T} \left(\frac{\gamma C_{\mathrm{V}}}{V_{\mathrm{m}}}\right)_{\mathrm{V}} \partial T \tag{2}$$

We employ the quasi-harmonic approximation (QHA) which states that the phonon frequencies are only a function of volume. Therefore the factor γ/V_{m} can be taken out of the integral for the thermal pressure, which becomes:

$$\Delta Pth = \frac{\gamma}{V_{\mathrm{m}}} \int_{T0}^{T} C_{\mathrm{V}} \partial T \tag{3}$$

For the final EoS of garnets we follow previous work (e.g. Stixrude and Lithgow-Bertelloni 2005; Gwanmesia et al. 2007; Kono et al. 2010; Hartwig and Galkin 2021) and use the MGD EoS in which the spectrum of thermally induced vibrations in the crystal is approximated by the Debye model for a single phonon whose energy distribution (dispersion) is represented by a characteristic temperature θ_{D}, the Debye temperature, corresponding to the maximum frequency of the phonon.The wavenumber in cm^{-1} of a phonon corresponding to the Debye temperature in K is $0.695\theta_{\mathrm{D}}$ and it's energy in meV is $0.086\theta_{\mathrm{D}}$. The heat capacity of a single phonon in the Debye model is then given by the third Debye function of the ratio $\left(\frac{\theta_{\mathrm{D}}}{T}\right)$. The heat capacity of the solid in the MGD EoS is then $3N$ times this value, there being $3N$ phonons in a mineral with N atoms in its formula unit.

For calculations at different volumes one has to account for the change in phonon energies as the volume varies. The coefficient relating these two quantities is strictly the mode Grüneisen parameter γ_i for each phonon mode:

$$\gamma_i = -\frac{\partial \ln \theta_{\mathrm{D}i}}{\partial \ln V} \tag{4}$$

Because in the MGD all of the phonons of the solid are represented by a single phonon, its γ_i is equal to γ. The simplest expression for the variation of γ consistent with the assumption of QHA is:

$$\gamma = \gamma_0 \left(\frac{V}{V_0}\right)^q \tag{5}$$

In which q is a constant and a refineable parameter of the EoS. By combining Eqs. (4) and (5) it follows that the Debye temperature varies as:

$$\theta_{\mathrm{D}} = \theta_{\mathrm{D0}} \exp\left(\frac{\gamma_0 - \gamma}{q}\right) \tag{6}$$

The parameters θ_{D0} and γ_0 are the values at the reference conditions. In refinements the values of θ_{D0}, q and γ_0 are usually highly correlated so that their values cannot be determined independently even when extensive datasets are available; for example Hartwig and Galkin (2021) had to fix the value of q to obtain values of θ_{D0} and γ_0 by refinement to thermal expansion data. We therefore apply a constraint to the MGD EoS (Kroll et al. 2019; Angel et al. 2020) that has recently been termed 'q-compromise' because the Debye temperature is kept constant, which implies that $\gamma = \gamma_0$ (Eq. 6) and therefore $q = 0$ (from Eq. 5), while the ratio γ/V is also kept constant which implies that $q = 1$ (Eq. 5). Careful reading of Holland and Powell (2011) reveals that their thermal-pressure EoS is also a q-compromise model (Kroll et al. 2012). The parameter q is therefore not a parameter in these q-compromise EoS, leaving θ_{D0} and γ_0 as refineable parameters. One of the characteristic properties of q-compromise EoS is that C_{V} is a function only of T and does not change with pressure. This means that the thermal pressure is also only a function of T, that the isochors are parallel to one another (but not linear), and that the isothermal bulk modulus K_{T} is constant along each isochor while the thermal expansion coefficient is not. The last makes intuitive physical sense because it implies that thermal expansion is purely a result of the dynamical motions of the atoms (leading to thermal pressure) while elastic stiffness, as represented by the bulk modulus, is solely a function of the average interatomic separations, and thus volume.

Data selection: Cp-EoS

One of the challenges in obtaining EoS parameters for a given mineral is deciding which volume and elasticity data or datasets are correct, or at least consistent with one another. By contrast, precise and accurate measurements of the isobaric heat capacity C_{p} for most garnets are available at room pressure (e.g. Geiger and Dachs 2018). Unfortunately these data cannot be used directly in the fits of EoS because the detailed evolution of C_{P} with T depends on details of

both the phonon density of states (e.g. Kieffer 1979; Ross 1992) and so-called 'non-lattice contributions' (e.g. Chopelas 2006) which are not modelled in EoS such as MGD. The C_p calculated from an MGD EoS is therefore typically larger than the experimental values (Fig. 1), meaning this comparison cannot be used to validate the EoS parameters nor to identify inconsistent data. The same is true for the thermal-pressure EoS of Holland and Powell (2011) in which the phonon density of states is represented by a single Einstein oscillator.

Therefore, we introduce a more direct approach in which we use experimental heat capacity data (C_P) to calculate the C_V of garnets, which is then be used in Eq. 3 to calculate ΔPth. The procedure is iterative; we make an estimate of the quantities in $(1+\alpha\gamma T)$ from an EoS fitted to some or all of the data and then use it to recalculate new values of C_V from

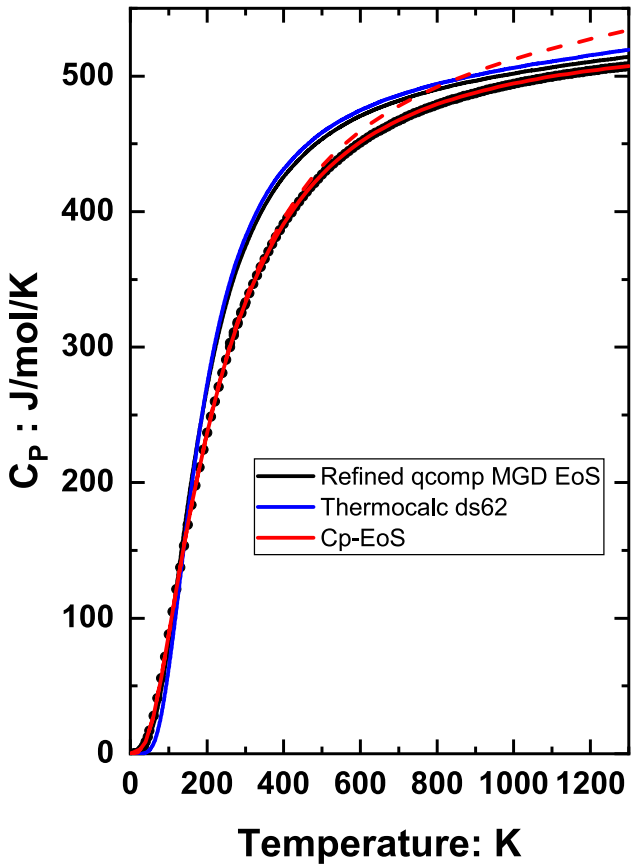

Fig. 1 Isobaric heat capacity C_P of grossular at room pressure. Data points are experimental data (Dachs et al. 2012b). The C_P calculated from the q-compromise MGD EoS fitted to volume and elasticity data is too high, as is that from the EoS from ds62 of Thermocalc (Holland and Powell 2011) because their phonon densities of state are over-simplified. When C_V is assumed equal to the experimental C_P, then the C_P calculated from the EoS is also overestimated (red dashed line). But just two cycles of EoS refinement and recalculation of $C_V = (1+\alpha\gamma T)^{-1}C_P$ leads to convergence of EoS parameters and agreement (solid red line) with the experimental C_P values.

C_P. Then we use the new C_V to calculate the thermal pressure during a new refinement of the other EoS parameters to the available data, which then provides new values of $(1+\alpha\gamma T)$ which can be used to do a new conversion of C_P to C_V. This cycle is repeated until the new calculated C_P matches the experimental values, and there is no further change in the refined values of the other EoS parameters. Even if the quantity $\alpha\gamma T$ is assumed to be zero at the start of this process (i.e. that $C_V = C_P$) then convergence is achieved in three or less iteration cycles (Fig. 1). Because we only have C_p data at room pressure, we have to make the assumption that $\left(\partial C_V/\partial P\right)_T = 0$, which is an equivalent approach to setting the θ_D in a MGD EoS constant (and thus $q=0$). But the thermal Grüneisen parameter γ still appears in the expression for thermal pressure (Eq. 3) and its variation with volume (Eq. 5) can still be described by a value of $q \neq 0$. In this paper we refer to EoS determined using the C_P data as 'Cp-EoS'.

This iterative procedure to obtain the Cp-EoS can be applied in several ways. One is to start with all of the available volume and elasticity data in the refinement of the EoS parameters, and to gradually remove those data or datasets that are inconsistent with the properties of the EoS. Or one can start with a minimum of data, or different subsets of the data, and then add additional data that are found to be consistent with the predictions of the EoS.

EoS refinement

Once an initial self-consistent set of data was identified with the help of the C_P data, these data were then fit with q-compromise MGD EoS which are more convenient in use because they do not require tables of C_V values, and they are not restricted in temperature by the temperature range of the heat capacity measurements. Fits were performed to the data for each individual garnet with the version of EosFit7c (Angel et al. 2014) that was released in summer 2021 (at www.rossangel.net and www.mineralogylab.com). EoS parameters are refined simultaneously to volume and moduli data using the methods described in Milani et al. (2017). The conversion between adiabatic and isothermal moduli, $K_S = (1+\alpha\gamma T)K_T$, is handled internally within the program, and the thermal Grüneisen parameter at reference conditions (γ_0) is a refinable parameter of the EoS. All fits were performed by weighted-least-squares to minimise the total sum of squared residuals in pressure $\sum w\left(P_{obs}-P_{calc}\right)^2$ summed over all of the data, with P_{calc} being the pressure calculated from the EoS at the experimental volume and temperature. The weight w of each individual data point is calculated from all of the experimental uncertainties in pressure, temperature *and* volume (or bulk modulus for elasticity data) by the effective variance method (Orear 1982).

Further technical details are provided in the help system of the EosFit program suite, and in Angel (2000) and Angel et al. (2014).

As analysis proceeded, further individual data points and datasets that were inconsistent with the majority of the data were sometimes identified. Scaling is meaningless for individual data, so aberrant individual data points were excluded. Justification can often be found in the description of the experiment when it indicates, for example, development of non-hydrostatic stresses at high pressure, or decomposition of the sample at high temperatures (e.g. Thiéblot et al. 1998). Where possible, inconsistent datasets were assigned a refineable scale factor, which was simultaneously refined with all of the EoS parameters to all of the data (Ehlers et al. 2022). The reliability of the refined value of each scale factor was evaluated in the light of the information given in the corresponding publication about the experiment. Because rescaling of one dataset can lead to previously aberrant data points in other datasets becoming consistent, we took care to re-review which data points were included and excluded at each step of the analysis and, in some cases, reinstated data into the refinements of the EoS and the consistency with C_P data was re-confirmed.

All bulk moduli and their pressure derivatives reported here are isothermal Reuss values, except where explicitly stated. The final refined parameters recommended for the *q*-compromise MGD EoS for each garnet are given in Table 1. Over the temperature range of the C_P data the *q*-compromise MGD EoS yield *P–V–T* behaviour for garnets that is indistinguishable from the Cp-EoS. The EoS parameters are also available as.eos files in the supplementary materials and at www.mineralogylab.com and www.rossangel.net. These files can be read directly into the EosFit software (Angel et al. 2014; Gonzalez-Platas et al. 2016) which enables a wide range of EoS calculations to be performed. The .eos files also include the variance–covariance matrix of the parameters from the final least-squares fit, from which the covariance of parameters are propagated into the uncertainties of any calculated property such as bulk modulus or volume.

Table 1 Parameters for BM3 + q-compromise MGD EoS of garnets

	Pyrope	Almandine	Spessartine	Grossular
V_0 (cm^3/mol)[a]	113.13	115.25	117.92	125.35
Fitted parameters				
K_{0T} (GPa)	169.3 (3)	174.6 (4)	177.57 (6)	167.0 (2)
K'_{0T}	4.55 (5)	5.41 (13)	4.6 (3)	5.07 (8)
θ_{D0}	771 (28)	862 (22)	860 (35)	750 (13)
γ_0	1.185 (12)	1.16 (fixed)	1.18 (3)	1.156 (6)
Derived values at 298 K				
K_{0S} (GPa)	170.7 (4)	175.8 (4)	178.77 (7)	168.2 (2)
$\alpha_V \times 10^{-5}$ (K^{-1})	2.256 (5)	1.957 (5)	1.919 (1)	2.047 (3)

[a]The values of V_0 are fixed parameters in this analysis, and were taken fromHolland and Powell (2011)

Garnet EoS

Grossular

In all thermal-pressure EoS the compressional EoS at room temperature is the basis for calculations of all high-temperature properties. Therefore, the initial step of the analysis is to establish the approximate parameters of the room-*T* EoS from *PV* data and determinations of K_S at pressure. As noted above, the values of pressure in the *PV* dataset of Milani et al. (2017) were rescaled to the quartz pressure scale of Scheidl et al. (2016). It is clear from Fig. 2 that the measurements of volume that form part of the results of the *PVT* measurements of Kono et al. (2010), Greaux et al. (2011) and Gwanmesia et al. (2014) are much more scattered than the pure *PV* datasets available (Table S1) although

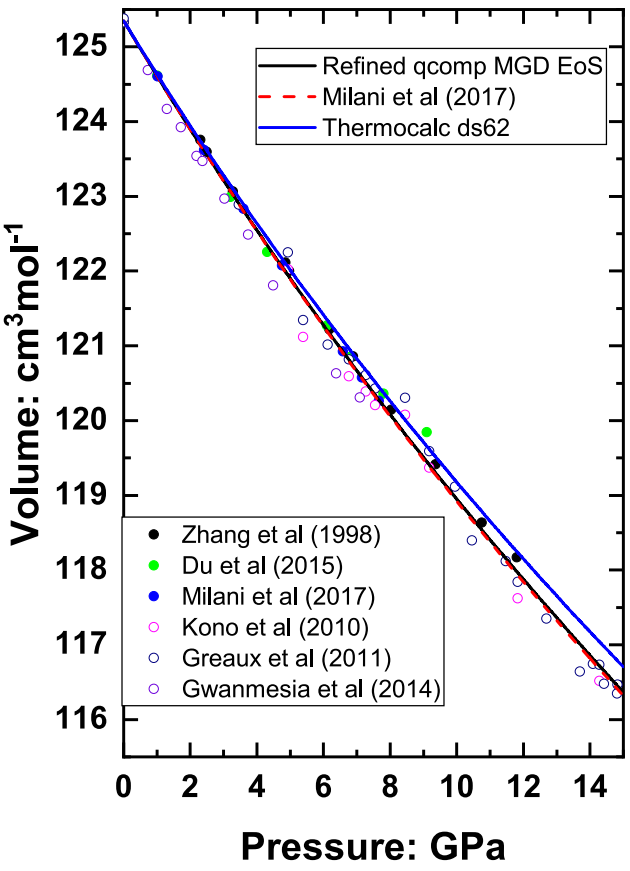

Fig. 2 Pressure–volume data for grossular at room temperature with fitted EoS. Note that the refined MGD EoS and that of Milani et al. (2017) overlap in this plot

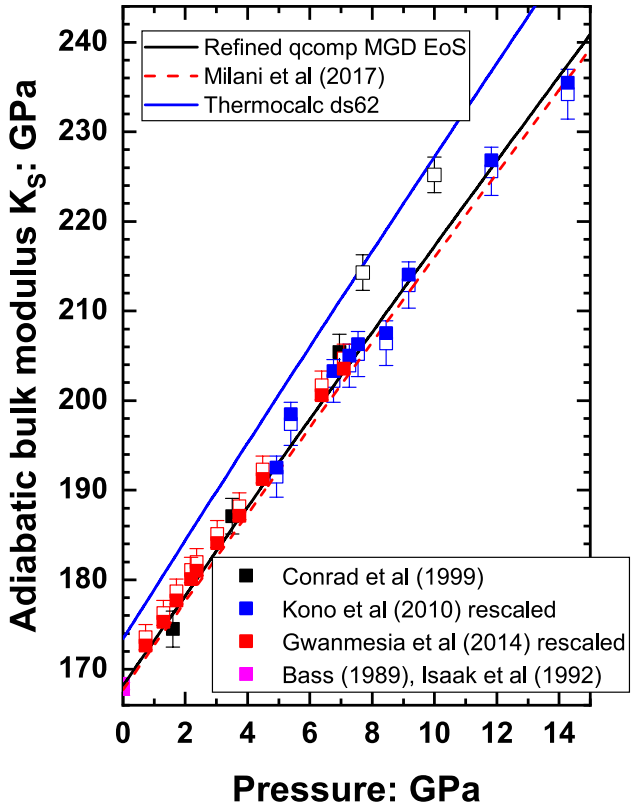

Fig. 3 Adiabatic bulk modulus data for grossular at room temperature. Solid symbols are the data used in the final fit of the EoS. The original data of Kono et al. (2010) and Gwanmesia et al. (2014) are shown as open symbols, the values multiplied by the scale factors obtained from the least-squares refinement are shown as solid symbols. The two highest pressure data of Conrad et al. (1999) were excluded from refinements as outliers

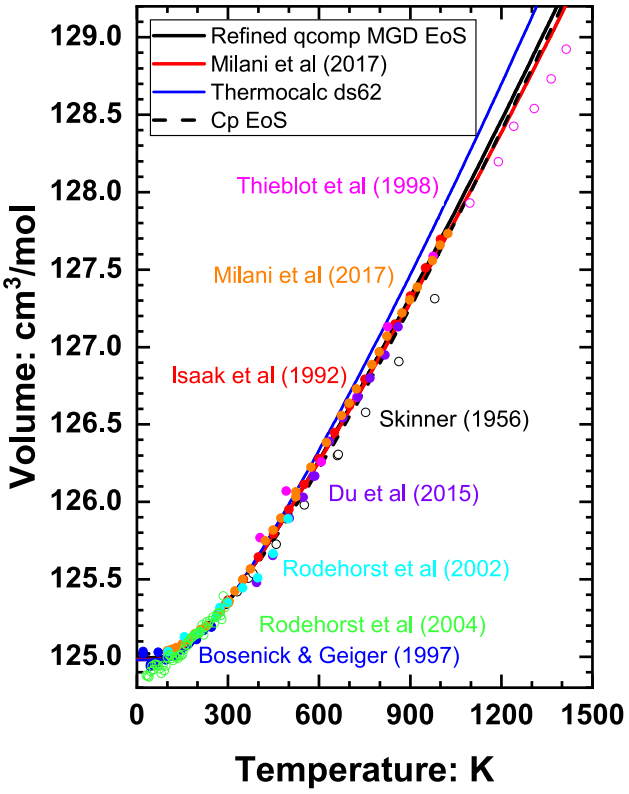

Fig. 4 Volume data for grossular at room pressure. Sources of data are indicated by the colours of the symbols and associated text labels. Note the data of data of Skinner (1956) and Thiéblot et al. (1998) are not consistent with the Cp-EoS (black dashed line), and are therefore inconsistent with the heat capacity data (Fig. 1)

they agree within the data scatter with the *PV* relationship defined by the more precise data shown in Figs. 2 and 3. Therefore, in the presence of direct determinations of bulk moduli at simultaneous high *P* and *T* from the latter two studies, the *PVT* data do not provide any significant additional constraints on the EoS, and were therefore excluded from further analysis. The high *P* elasticity data of Kono et al. (2010) and Gwanmesia et al. (2014) appear (open symbols in Fig. 3) to be mutually inconsistent; the moduli from Kono et al. (2010) consistently fall below the trend defined by the data of Gwanmesia et al. (2014). The underlying reason for this discrepancy is not apparent from the published papers. Given that one cannot determine a-priori which of these datasets is correct, we refined scale factors to both of these datasets during the fit of the EoS parameters to all of the data for grossular. This yields a single EoS that fits both these scaled data (solid symbols in Fig. 3) and the volume compression data (Fig. 2).

The EoS parameters cannot be determined from the elasticity data alone because the lack of data below 300 K means that the value of the Debye temperature is not constrained. Therefore, *V*–*T* data, particularly at low *T*, are essential to determine the parameters of the MGD EoS. However, the published *V*–*T* datasets show significant differences, both at low and high temperatures (Fig. 4). The Cp-EoS based on the heat capacity data of Dachs et al. (2012b) and refined to the all the available elasticity data as well as the *P*–*V* data at room temperature (and *not* any *V*–*T* data) clearly shows (Fig. 4) that the low-*T* data of Rodehorst et al. (2004) and the high-*T* data of Skinner (1956) and Thiéblot et al. (1998) are inconsistent with all the other data for heat capacity and elasticity of grossular. All three datasets were therefore excluded from all further EoS fits. The deviation of the data of Thiéblot et al. (1998) above 1000 K may indicate the start of the decomposition detected by the authors at higher temperatures, or a problem with their temperature calibration. The reason for the low values of *V* (or overestimate of *T*) in the data of Skinner (1956) is not clear; a similar offset is apparent in his data for pyrope, but not for spessartine.

Initial refinements of the EoS parameters also led to large misfits to the *PV* data of Zhang et al. (1999) and Du et al. (2015), much larger than the estimated uncertainties in the

Table 2 Parameters for BM3 + full MGD EoS of garnets

	Pyrope	Grossular
V_0 (cm^3/mol)[a]	113.13	125.35
Fitted parameters		
K_{0T} (GPa)	169.4 (3)	167.3 (2)
K'_{0T}	4.55 (5)	5.07 (5)
θ_{D0}	771 (28)	748 (13)
γ_0	1.185 (12)	1.157 (5)
q	0.79 (17)	0.84 (12)
Derived values at 298 K		
K_{0S} (GPa)	170.7 (4)	168.5 (3)
$\alpha_V \times 10^{-5}$ (K^{-1})	2.256 (5)	2.047 (3)

[a]The values of V_0 are fixed parameters in this analysis, and were taken from Holland and Powell (2011)

data. These data were therefore also excluded from final refinements. The exclusion of this data does not significantly affect the *PVT* behaviour predicted by the refined EoS, but it does lead to reduced uncertainties in the individual parameter values. A total of 106 volume data and 114 bulk modulus data were used in the final refinements (Table S1).

Refinement of the parameter q in a full MGD EoS to these data yields a value of 0.84(12), Table 2, which lies between the values of 0 and 1 that are the 'implied values' for different components of the q-compromise EoS. Therefore, refinement of the q-compromise and full MGD models yields indistinguishable values for all of the other EoS parameters for grossular, and the properties predicted by the two EoS at high P and T are therefore also indistinguishable. We therefore only show the results with the q-compromise version (Table 1). The refined scale factors for the two large datasets of K_S data are 0.995(4) for the data of Kono et al. (2010), indicating that, on average, the experimental values are too small by 0.5% compared to the values predicted from an EoS fitted to all of the other data. In contrast, the scale factor of 1.006(3) suggests that the K_S values of Gwanmesia et al. (2014) are too large by 0.6%, which is consistent with the pattern of data collected at room T and high pressure (Fig. 3). Both scale factors may arise from a number of experimental causes as we have discussed above in the "Methods" section.

As can be seen in Figs. 2, 3 and 4 the refined q-compromise MGD EoS reproduces all of the consistent measured volume and elasticity data on grossular to within the experimental uncertainties, with the possible exception (Fig. 5) of the slight decrease above 900 K in dK_S/dT marginally suggested by the data. The compressional properties of the new q-compromise MGD EoS for grossular are indistinguishable from those of Milani et al. (2017), because of their use of elasticity data to constrain the EoS parameters. The EoS from Thermocalc ds62 (Holland and Powell 2011) has a

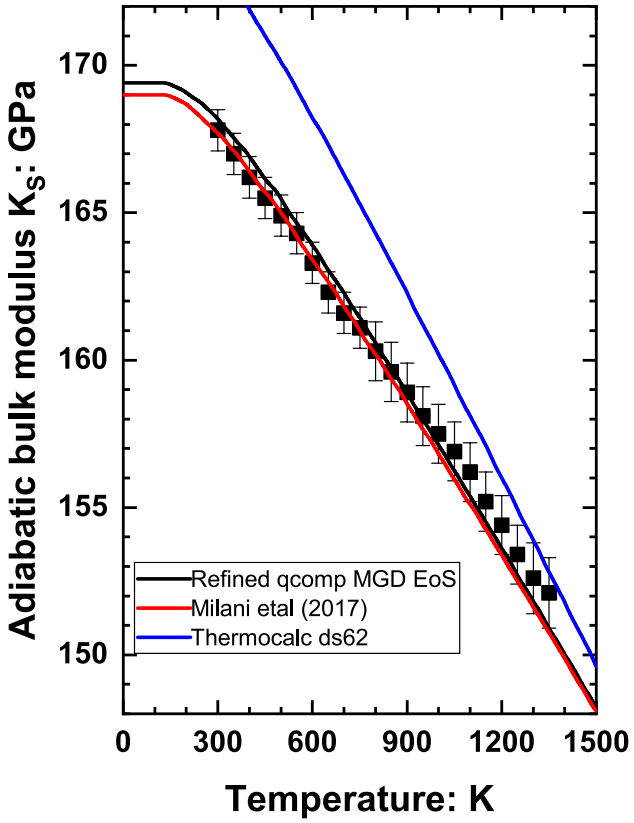

Fig. 5 The variation of K_S of grossular with temperature predicted by EoS (lines) and the data of Isaak et al. (1992). The Cp-EoS is indistinguishable from the q-compromise MGD EoS. The Thermocalc EoS has a value of K_{S0} that is too large. None of the EoS predict the slight decrease in dK_S/dT visible in the data above 900 K

higher value of the bulk modulus at all conditions (Figs. 2, 3, 5), primarily as a result of a significantly stiffer $K_{T0} = 172$ GPa, which is not consistent with several elasticity datasets, and a higher value of $K'_{T0} = 5.53$.

The consequence for piezobarometry is that the isomekes of grossular with α-quartz (Fig. 6a) calculated with the new MGD EoS and the EoS of Milani et al. (2017) are indistinguishable on the scale of measurement uncertainties but those calculated with the Thermocalc EoS lie at pressures 0.1–0.2 GPa lower for the same remnant inclusion pressure. In the stability field of β-quartz where the isomekes are steeper and act as a geothermometer, the Thermocalc EoS predicts entrapment temperatures ~ 80 K lower than the new MGD EoS.

The difference between the bulk moduli of zircon and garnets is much less than that between garnets and quartz and therefore the isomekes of zircon with garnet have steeper slopes dP/dT and the residual pressures of zircon inclusions are best used as a geothermometer. The positions of the entrapment isomekes (Fig. 6b) are very sensitive to the thermal expansion coefficients of the two phases. Thus, although

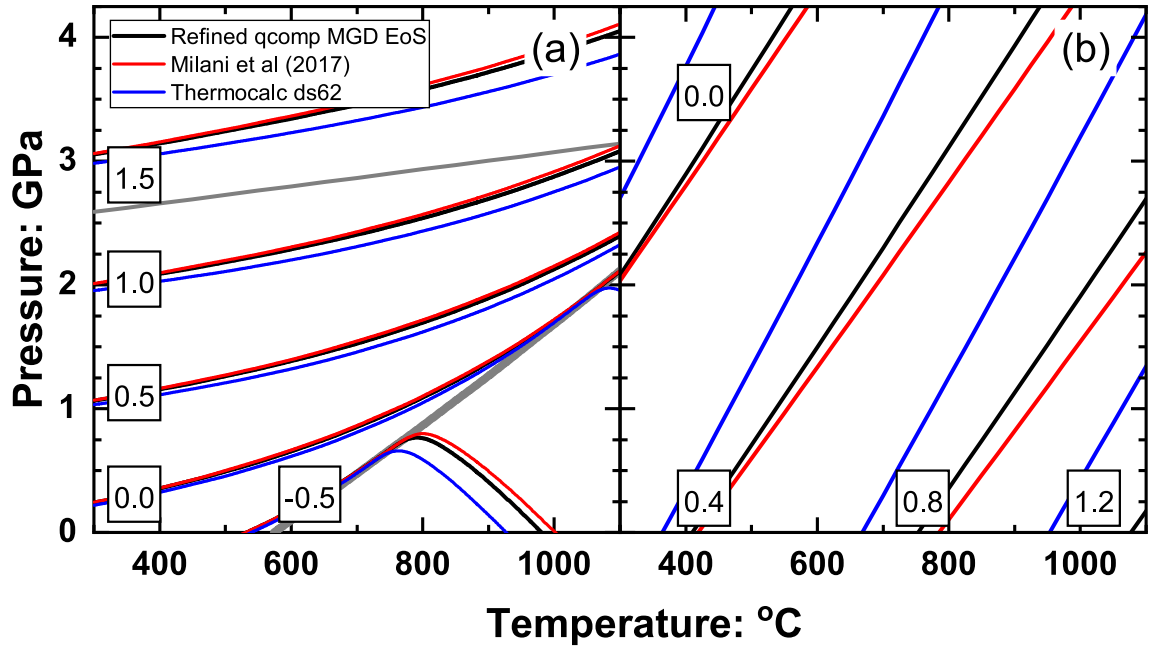

Fig. 6 **a** Entrapment isomekes of quartz (Angel et al. 2017a) with grossular for different grossular EoS. The two grey lines are the phase boundaries for α-quartz = coesite (Bose and Ganguly 1995) and $\alpha = \beta$ quartz. **b** Isomekes of zircon (Ehlers et al. 2022) with different grossular EoS. Numbers in boxes are the inclusion pressures in GPa that would be measured at room conditions for inclusions trapped on the isomekes

the differences in the thermal expansion predicted by the EoS from Thermocalc ds62 (Holland and Powell 2011), the new MGD EoS, and that of Milani et al. (2017) appear small (Fig. 4), the isomekes for a given residual inclusion pressure diverge significantly. For example, a zircon trapped under UHP conditions at 3.0 GPa and exhibiting a residual pressure of 0.4 GPa would imply entrapment of 665 °C from the Thermocalc EoS, 825 °C from that of Milani et al. (2017) and 785 °C with the new q-compromise MGD EoS for grossular (Fig. 6b).

Pyrope

Most of the datasets on the elastic properties and *PVT* behaviour of pyrope published prior to 1990 have been superceded by more precise measurements and were therefore not considered further. With the rapid increase in data available for end-member pyrope (Table S2) we were able to exclude from our analyses measurements on near-end-member composition natural garnets, such as those from the Dora Maira locality. These data can be used subsequently to determine the effects of minor solid solution components on the elastic properties of pyropes.

The *PV* data at room *T* of Leger et al. (1990) show much large uncertainties and larger data scatter than other room-*T* data, perhaps arising from the use of a solid pressure medium. The room-*T* *PV* data of Gwanmesia et al. (2006) also have larger scatter compared to other studies, so neither dataset significantly constrains the EoS parameters in the presence of more precise data (Fig. 7). They were therefore excluded. Unfortunately, the wave velocity data from Chen et al. (1999) cannot be used as they determined compressional and shear wave velocities in different experiments at different pressures. The values of K_S of Sinogeikin and Bass (2000) are systematically low compared to other data (Fig. 8), as previously noted (Chantel et al. 2016), and were assigned a refineable scale factor; its refined value of 0.978(6) indicates that the discrepancy is ca. 2% on average.

As for grossular, the published *V*–*T* data of pyrope show different trends at low temperatures, and the data of Skinner (1956) and Thiéblot et al. (1998) indicate significantly lower thermal expansion at high temperatures than the other data. The Cp-EoS refined to the *P*–*V* and the elasticity data clearly shows (Fig. 9) that only the data of Hartwig and Galkin (2021) and Milani et al. (2015) are consistent with the heat capacity data (Bosenick et al. 1996; Dachs and Geiger 2006). With the addition of these two *V*–*T* datasets (Table S2), the Cp-EoS gives $q = 1.10(16)$, indicating that q for the thermal Grüneisen parameter (Eqs. 3, 5) is 1 within uncertainties, consistent with a q-compromise model for the thermal pressure. This is confirmed by the fit of a full MGD EoS which gave a value of $q = 0.79(17)$ with $\chi^2_w = 2.23$ (Table 2). A refinement of a q-compromise MGD EoS provides identical EoS

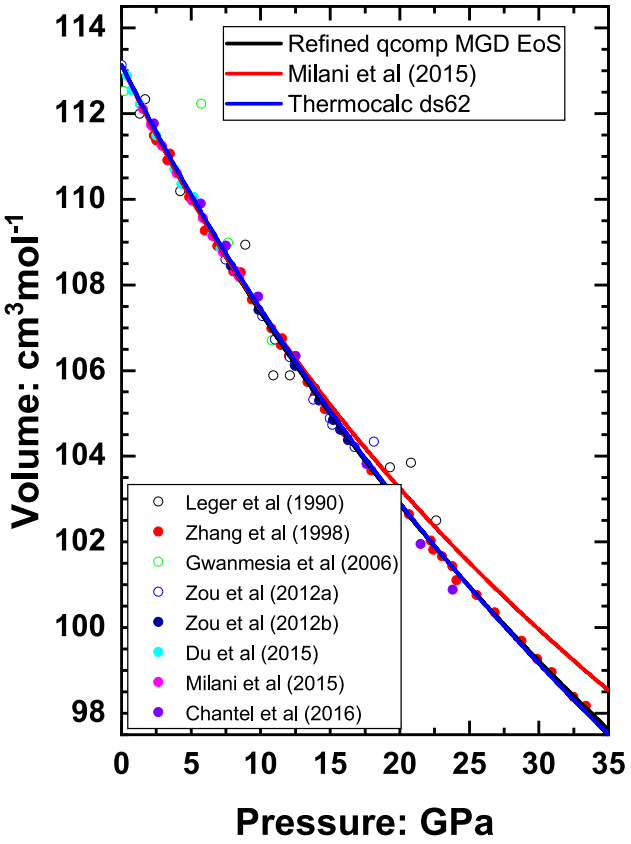

Fig. 7 Pressure–volume data for pyrope at room temperature with fitted EoS. The EoS of Milani et al. (2015) diverges to larger volumes because it has a higher value of $K'_{0T} = 6.4(4)$

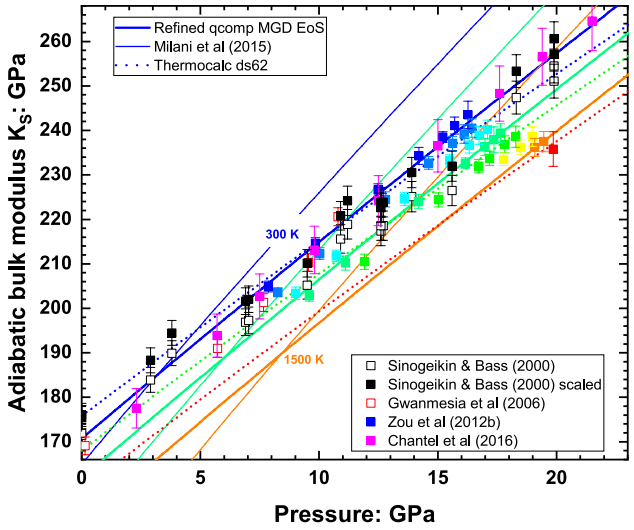

Fig. 8 Adiabatic bulk modulus data for pyrope at various temperatures. Solid symbols are the data used in the final fit of the EoS; the data of Sinogeikin and Bass (2000) are shown scaled by the refined scale factor. The corresponding original data are shown as open symbols. The high-temperature data (Zou et al. 2012b) and EoS lines (at 300, 900 and 1500 K) are colour-coded by temperature. Note that spacing of the isotherms of all of the EoS are approximately the same as the data. This indicates that the EoS of Milani et al. (2015) has the correct temperature dependence $\left(\partial K_S/\partial T\right)_P$, but a higher value of K'

parameters (Table 1), including values of θ_{D0} and γ_0 and almost as good quality of fit to the data ($\chi^2_w = 2.24$), confirming the conclusion from the analysis of grossular that q-compromise EoS are adequate for describing the volume (Figs. 7, 9) and elasticity variation of garnets with P and T, including the measured variation of adiabatic bulk modulus with T both at ambient and high pressures (Fig. 8).

In particular, the fit of this q-compromise EoS to the data clearly indicates that the determinations of bulk moduli at high T and ambient P (Sinogeikin and Bass 2002) are consistent with all of the other data that were included. Therefore, we conclude that the values of bulk moduli determined at 0.3 GPa by Gwanmesia et al. (2007) must be in error because they are lower than the values measured at ambient pressure by Sinogeikin and Bass (2002). The high P, T bulk moduli data from Gwanmesia et al. (2006) agree with those predicted from the refined EoS but have much larger data scatter than the later measurements of Zou et al. (2012b), so their addition to the refinement does not significantly change the refined EoS parameters nor reduce the parameter uncertainties. The same applies to the PVT datasets (Gwanmesia et al. 2006; Zou et al. 2012a, 2012b; Chantel et al. 2016) because the high-PT elasticity data provide such strong constraints on the parameters of the EoS.

Figures 7, 8 and 9 show that the new q-compromise MGD EoS has very similar properties to the Cp-EoS and that from ds62 of Thermocalc (Holland and Powell 2011), and there are only small differences in their predicted properties, including bulk modulus, at simultaneous high P and T (Fig. 8), arising from the availability of the data of Zou et al. (2012b) for the current refinement. In contrast, it is obvious that the EoS of Milani et al. (2015) has a $K_{0T} = 163.7(1.7)$ GPa that is too low and $K'_{0T} = 6.4(4)$ that is too high, compared to available elasticity data. This was due to the normal correlation of K_0 and K'_{0T} in refinements to data of limited P range, the study using the old calibration of the quartz PV EoS (Angel et al. 1997), and not using the available elastic data because fitting of them had not yet been developed in EosFit.

The isomekes of pyrope with quartz and zircon of the new EoS are very similar to those of the EoS from Thermocalc ds62 (Fig. 10), whereas those for quartz with the pyrope EoS of Milani et al. (2015) lie 0.1 GPa higher at UHP conditions, and at higher temperatures in the stability field of β-quartz. The differences of the Milani et al. (2015) EoS isomekes with zircon from other EoS are larger primarily because it has a softer bulk modulus at low pressures leading to a less negative isomeke pressure

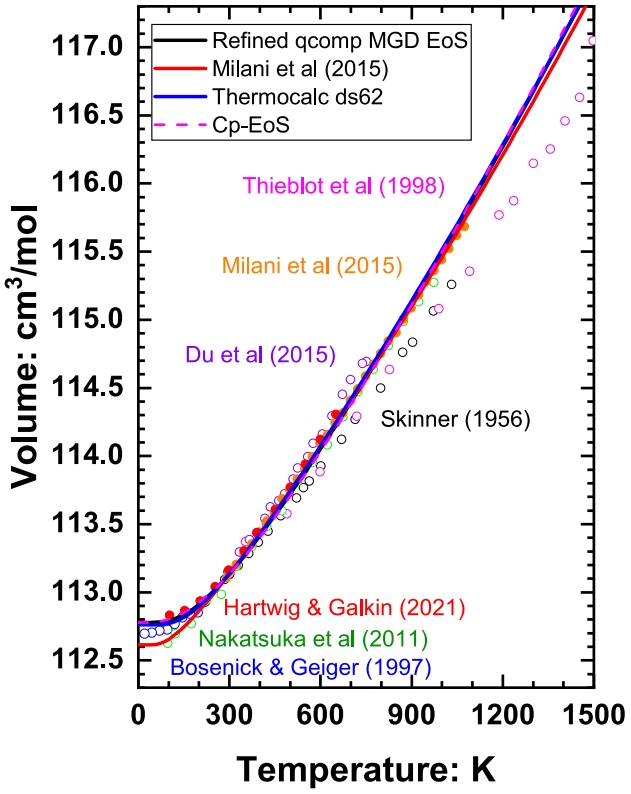

Fig. 9 Volume data for pyrope at room pressure. The data represented by open symbols are not consistent with the heat capacity data (Bosenick et al. 1996; Dachs and Geiger 2006) represented by the line for the Cp-EoS. The thermal expansion of the Milani et al. (2015) EoS is only significantly different from the others below room temperature

at room temperature and a shallower slope dP/dT of the isomekes (Fig. 10b).

Spessartine

The room-temperature compression data for spessartine are shown in Fig. 11. It is clear that the data of Leger et al. (1990) are scattered and do not contribute to constraining the EoS parameters, so they were not used in any fits. The data of Gréaux and Yamada (2014) are very slightly systematically lower in volume than the other datasets, and that of Zhang et al. (1999) systematically higher. This indicates a minor inconsistency between the high-pressure data in each study and the reported value of V_0 at room pressure. This was accommodated in refinements by assigning scale factors to these datasets, whose final refined values of respectively 1.002 and 0.9995 confirm what can be seen in Fig. 11.

The only direct measurement of the elasticity of spessartine was at room conditions (Bass 1989), and therefore the thermal part of the EoS is only constrained by V–T data at room pressure in several studies plus the PVT data reported by Gréaux and Yamada (2014). Consequently, the parameters of the thermal part of the EoS of spessartine are very sensitive to these data. Unfortunately, close inspection of the only extensive dataset at low temperatures (Rodehorst et al. 2004) reveals a step in the V–T curve between 140 and 145 K (Fig. 12). This is not related to the lambda-type transition in spessartine at 6.2 K which has been interpreted as a Néel transition (Dachs et al. 2009). Neither does the heat capacity

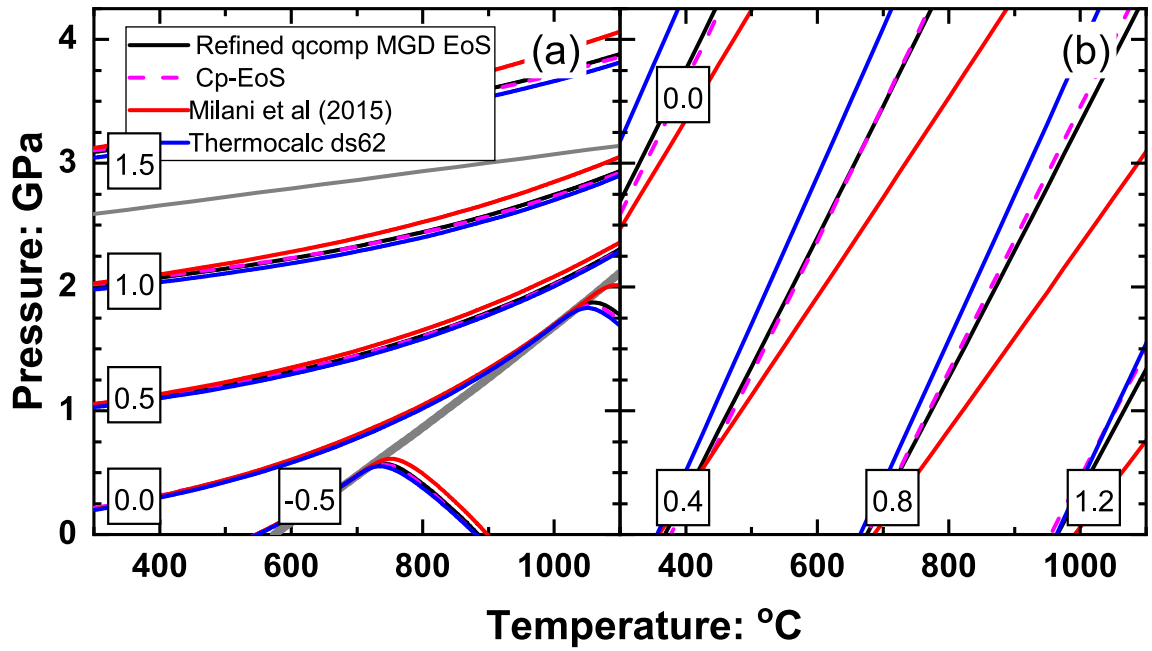

Fig. 10 **a** Entrapment isomekes of quartz (Angel et al. 2017a) with pyrope for different pyrope EoS. The two grey lines are the phase boundaries for α-quartz=coesite (Bose and Ganguly 1995) and $\alpha = \beta$ quartz. **b** Isomekes of zircon (Ehlers et al. 2022) with different pyrope EoS. Numbers in boxes are the inclusion pressures in GPa that would be measured at room conditions for inclusions trapped on the isomekes

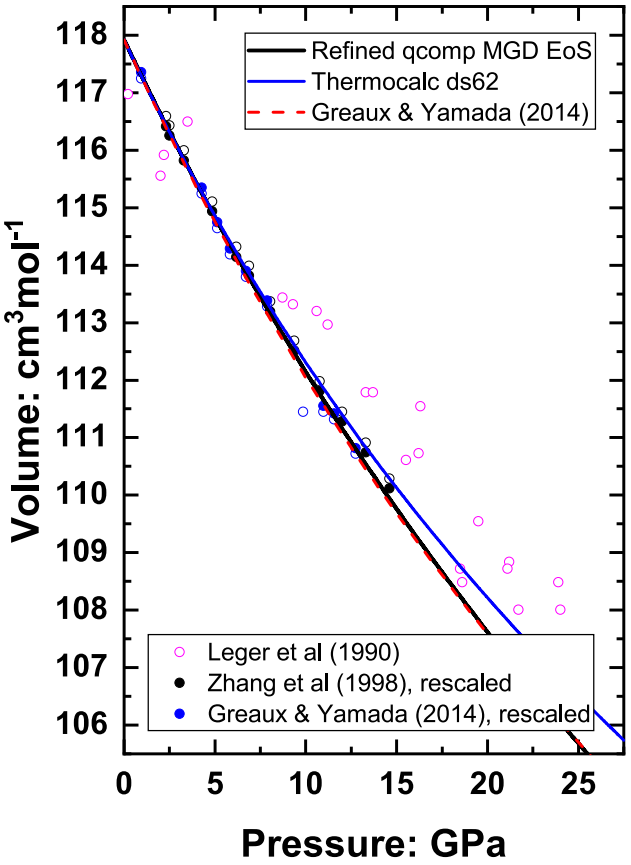

Fig. 11 Pressure–volume data for spessartine at room temperature with fitted EoS. Solid symbols are the data scaled by their refined scale factors. The corresponding unscaled original data are shown as open symbols. Note that the refined MGD EoS and that of Gréaux and Yamada (2014) overlap in this plot

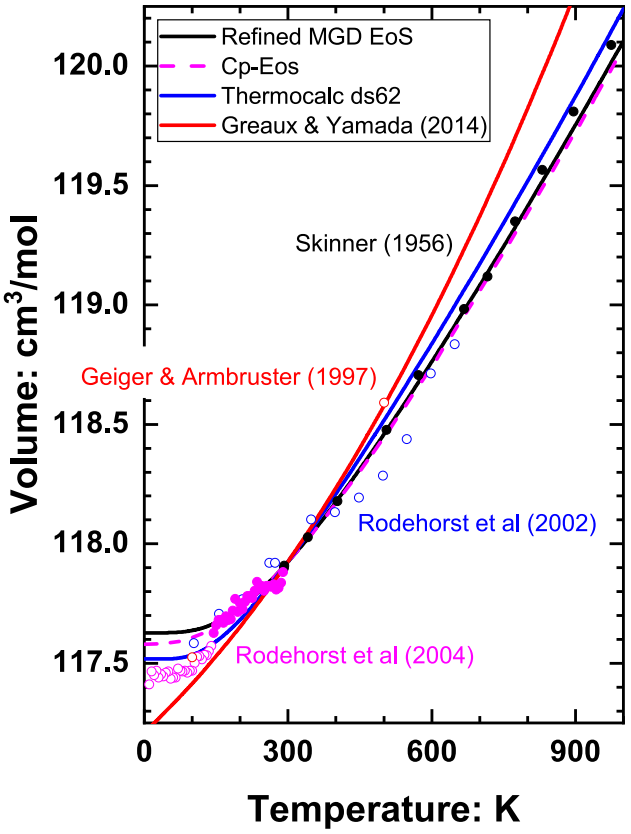

Fig. 12 Volume data for spessartine at room pressure. Sources of data are indicated by the colours of the symbols and associated text labels, with open symbols indicating data excluded from the final refinement. Note the step in the data of Rodehorst et al. (2004) at 140–145 K. The Cp-EoS indicates that the higher T data of Rodehorst et al. (2004) and the data of Skinner (1956) are consistent with the heat capacity data (Dachs et al. 2009)

data have any signature of a transition in the 140–150 K range in which the volume data exhibit a step. The Cp-EoS fitted to the elasticity datum and all consistent high-P volume data clearly show (Fig. 12) that the data of Rodehorst et al. (2004) below 145 K are inconsistent and suggest that the data of Skinner (1956) are consistent with the heat capacity. The latter is surprising in the light of the Skinner (1956) data for pyrope and grossular being at too high temperatures, but this conclusion for spessartine strongly depends on the value of single measurement of the adiabatic bulk modulus (Bass 1989) as that is the biggest control on the value of γ. But stable refinements can only be obtained by over-weighting this single datum, effectively forcing the EoS to reproduce the experimental value. The available data do not constrain the value of q at all, so q-compromise EoS were used throughout. The refined q-compromise MGD EoS (Table 1) returns indistinguishable volumes and bulk moduli at P and T from the Cp-EoS.

Although the PVT properties and isomekes calculated with the new q-compromise EoS for spessartine are similar to those of grossular, the EoS should be considered provisional. It is probably close to the truth, but new thermal expansion data at high-T and in-situ high-T or high-PT elasticity measurements are needed to confirm it. It has a higher value of K_{T0} and smaller K'_{T0} compared to the EoS of Gréaux and Yamada (2014) and the two EoS therefore predict indistinguishable PV curves (Fig. 11). The significantly higher value of K'_{T0} of the EoS from Thermocalc ds62 fits the original unscaled data of Zhang et al. (1999) and thus predicts larger volumes than the current EoS at high pressures. The EoS of Gréaux and Yamada (2014) does not fit the available volume data at any temperature (Fig. 12), probably because they did not use any room-pressure data to constrain their analysis. The volumes of these three EoS also diverge significantly below ~ 300 K (Fig. 12), so the values of the thermal expansion coefficient at room conditions differ by about 20% between them, reinforcing the conclusion that precise and

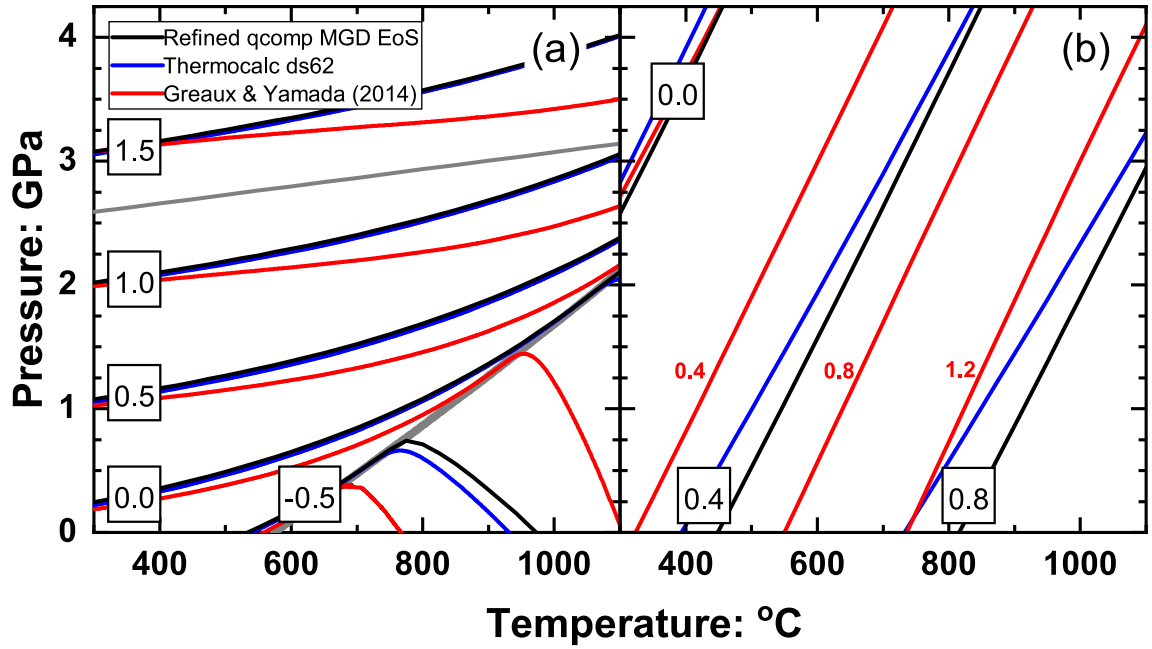

Fig. 13 **a** Entrapment isomekes of quartz (Angel et al. 2017a) with spessartine for different EoS. The two grey lines are the phase boundaries for α-quartz = coesite (Bose and Ganguly 1995) and $\alpha = \beta$ quartz. **b** Isomekes of zircon (Ehlers et al. 2022) with different spessartine EoS. Numbers in boxes are the inclusion pressures in GPa that would be measured at room conditions for inclusions trapped on the isomekes; in part **b** the inclusion pressures for the Gréaux and Yamada (2014) EoS are given by the small red numbers

accurate low-temperature data are essential for constraining the EoS of garnets at room conditions.

The similarities of the q-compromise MGD EoS and that from Thermocalc ds62 mean that their isomekes with quartz are indistinguishable, and with zircon differ only by 30 °C in predicted entrapment temperatures at metamorphic conditions (Fig. 13). The importance of an accurate description of the thermal expansion of garnets for piezobarometry is illustrated in Fig. 13 by the isomekes calculated for the spessartine EoS of Gréaux and Yamada (2014). Their isomekes with α-quartz are at significantly lower pressures and therefore cross the α–β transition at much lower P and T, with the result that in the stability field of β-quartz they lie ca. 200 °C lower than the other EoS (Fig. 13a). Similarly the isomekes of the Gréaux and Yamada (2014) EoS with zircon are ca. 150 °C lower than the other EoS (Fig. 13b).

Almandine

As for the other garnets, the PV part of the EoS at room temperature is reasonably well constrained by data (Fig. 14) from Milani et al. (2015) and the data collected with a helium pressure medium by Zhang et al. (1999), but the latter's data collected in a neon pressure medium are about 0.1% larger in volume. The same is seen with the data for spessartine (see above) and confirms that there is an inconsistency between the 'neon' data at high pressure and the room-pressure datum in these datasets of Zhang et al. (1999). The multi-anvil diffraction data of Arimoto et al. (2015) is too scattered to significantly constrain the EoS parameters and were omitted from all EoS fits. When refined with a scale factor for the neon data of Zhang et al. (1999) the single-crystal data together (Fig. 14) define the room-pressure bulk modulus as $K_{T0} = 174.1(6)$ GPa, consistent with the room-pressure adiabatic bulk modulus $K_{S0} = 175.6(1.8)$ GPa measured by Arimoto et al. (2015). However, this value is not consistent with the bulk moduli at simultaneous high P and T determined from wave velocity measurements (Arimoto et al. 2015), so a scale factor was applied to the latter during all EoS refinements.

Figure 15 shows that the only volume measurement of almandine below room temperature (Armbruster et al. 1992) is inconsistent with the curvature in the only high temperature measurements (Skinner 1956). The only further constraints on the thermal pressure are the high-PT elasticity data of Arimoto et al. (2015). Each one of these datasets can be made consistent with the experimental heat capacity data (Dachs et al. 2012a) but require very different EoS parameters, so which set of data and which set of parameters is correct is not clearly indicated by the Cp-EoS. We have therefore derived an EoS for almandine by constraining some EoS parameters so that the thermal behaviour is similar to the other garnets, and by evaluating the influence of each of the few datasets with extra care.

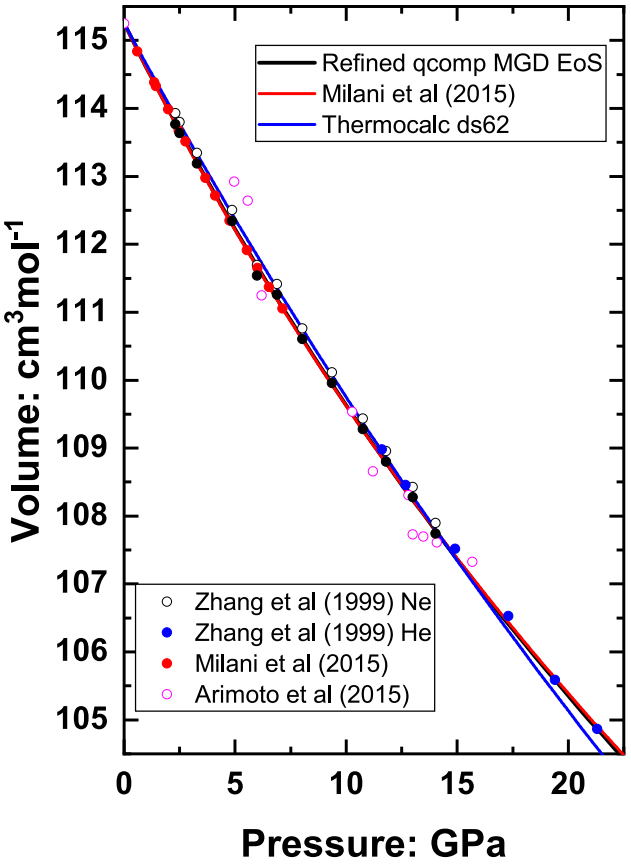

Fig. 14 Pressure–volume data for almandine at room temperature with fitted EoS. Solid symbols are the data used in the final fit of the EoS with the neon data of Zhang et al. (1999) shown multiplied by the refined scale factor from least-squares. Their unscaled original data are shown as open symbols

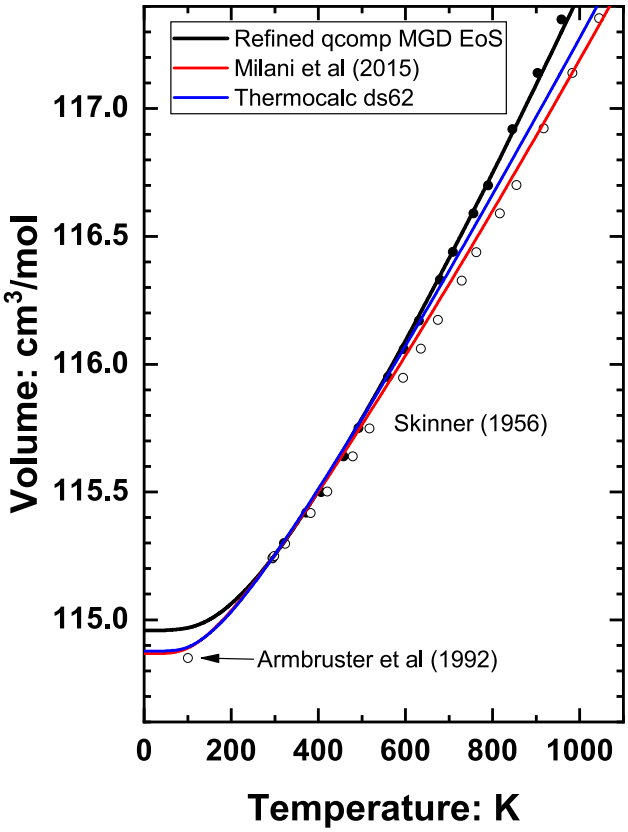

Fig. 15 Volume data for almandine at room pressure. Note that the curvature in the original data (open symbols) of Skinner (1956) is inconsistent with the only datum below room temperature (Armbruster et al. 1992). Solid symbols are the data of Skinner (1956) shifted as $T=0.8837\ T+34.7$ (all K) based on pyrope and grossular data

In combination with the heat capacity data, the V–T data of Skinner (1956) lead to values of $\gamma_0 = 1.00(1)$ which is much lower than other garnets, and this leads to a room-temperature thermal expansion coefficient (1.68×10^{-5} K^{-1}) that is also much lower. Therefore the heat capacity data (Dachs et al. 2012a) and elasticity data (Arimoto et al. 2015) demonstrate that the thermal expansion cannot be as low as suggested by the data of Skinner (1956). More reasonable values of $\gamma_0 = 1.16(1)$ and $\alpha_0 = 1.94\times10^{-5}$ are obtained if the data of Skinner (1956) are shifted down in temperature by $T=0.8837\ T+34.7$ (all K), a correction based on his pyrope and grossular data. This temperature correction corresponds to 70 K at 900 K.

Even with a scale factor, the elastic data of Arimoto et al. (2015) above 1100 K (at high P) can only be made consistent with the heat capacity data if the value of q is set to significantly greater than 1. This is in contrast to the other three garnets, but there are no obvious reasons in the heat capacity data for garnets as to why almandine should be different. We therefore assumed that the highest T data of Arimoto et al. (2015) may be in error, perhaps simply from some uncertainty or error in T measurement in their multi-anvil, so the data at 1300–1700 K were excluded. With these adjustments to the data of Skinner (1956) and only using the data at 1100 K and lower of Arimoto et al. (2015), one can refine a q-compromise MGD EoS to obtain γ_0 of 1.16–1.18 and θ_D between 850 and 920 K. These parameters are 96% correlated in the refinement so we fixed $\gamma_0 = 1.16$, similar to the other garnets, with which θ_D refines to 862(22) K (Table 1).

This EoS has low-temperature behaviour that is close to spessartine which seems reasonable because these two garnets are related by exchange of Fe and Mn on the dodecahedral site of the structure. But, given the lack of data and the consequent assumptions made in the analysis, this EoS must be regarded as provisional. It predicts properties (Figs. 14, 16) that are very similar to the EoS of Milani et al. (2015) at intermediate temperatures, but larger volumes and lower bulk moduli at high temperatures. Thus, the isomekes of these two EoS with α-quartz are similar but the q-compromise MGD EoS predicts significantly

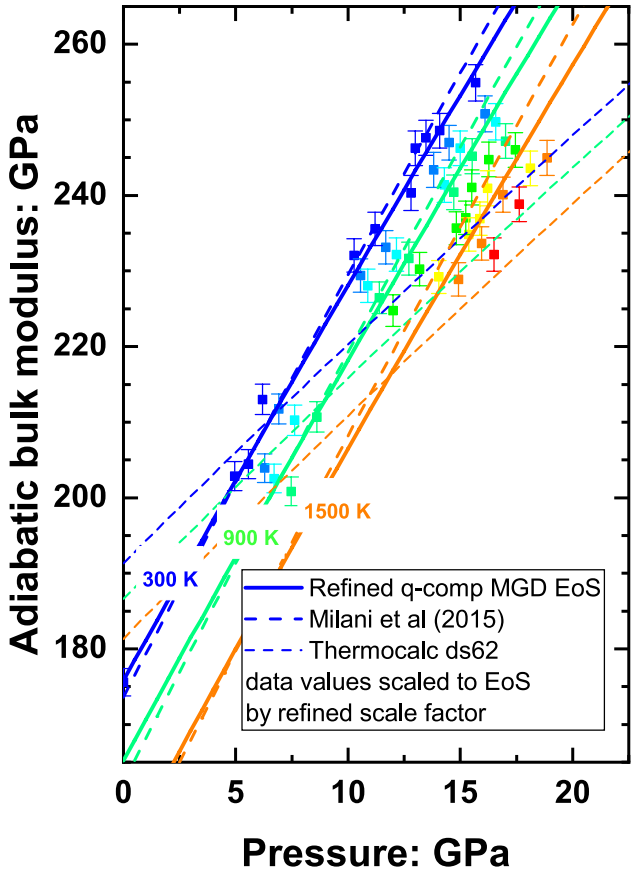

Fig. 16 Variation of the adiabatic bulk modulus of almandine with P and T. Data points (Arimoto et al. 2015) are shown rescaled by the refined scale factor of 0.945, except for the room P datum. Lines and data points are colour coded by temperature

lower inclusion entrapment temperatures for both β-quartz and zircon (Fig. 17). The Thermocalc ds62 EoS for almandine has an unrealistic large value of $K_{0T} = 190$ GPa and small $K'_{T0} = 2.98$ that appear to derive from a fit to the PV data of Zhang et al. (1999) collected in the neon pressure medium (Fig. 14), and is clearly inconsistent (Fig. 16) with the high P–T elasticity data of Arimoto et al. (2015).

Isomekes

Although there are no obvious trends in the values of individual EoS parameters with composition or molar volume (Table 1) the isomekes of the four end-member garnets calculated with the new q-compromise MGD EoS are much more similar to one another than those calculated with previous groups of garnet EoS, such as from Thermocalc (Holland and Powell 2011) or Milani et al. (2015, 2017). The isomekes of the new EoS (Fig. 18) with α-quartz and zircon are all close together at low temperatures because of the small range of the bulk moduli of the garnets compared to the contrast with the bulk moduli of quartz or zircon. The divergence of the isomekes towards higher T is then due to the differences in thermal expansion behaviour of the garnets, with those of pyrope diverging most because it has the largest and most different thermal expansion coefficient (Table 1). At low pressures and high temperatures the order of the isomekes for all garnets follows the trend in the garnet thermal expansion coefficients (Fig. 18) with the isomekes with pyrope lying at the lowest temperatures for a given inclusion pressure. Given that the EoS of grossular and pyrope are very well constrained by the elasticity and volume data, these systematics in the isomekes are an argument in support of the validity of the less well-constrained q-compromise MGD EoS of spessartine and almandine.

Inclusions of quartz in almandine have been synthesised at two known conditions in a piston cylinder (Bonazzi et al. 2019). Back-calculation of the entrapment isomekes from remnant inclusion pressures measured by Raman (Angel et al. 2019; Bonazzi et al. 2019) can then provide an indication of the accuracy of EoS for almandine. The almandine EoS from Thermocalc (Holland and Powell 2011), Milani et al. (2015) and the current work (Table 1) all yield intrinsic uncertainties in the entrapment pressures of about ± 0.05 GPa at high temperatures, and all pass within the estimated absolute uncertainty in the pressure calibration of the piston cylinder apparatus (Fig. 19). At these conditions the isomekes of the MGD EoS are indistinguishable from those of the Thermocalc EoS and both suggest lower entrapment pressures than the recorded pressure of synthesis. This discrepancy may arise from the volume change of the sample during the reactions that formed garnet and quartz from the starting materials, and from the effects of inclusion shapes, the uncertainties of Raman measurements, and the use of room-pressure elastic moduli (Bonazzi et al. 2019; Gilio et al. 2021; Mazzucchelli et al. 2021) in the calculation of the remnant inclusion pressures.

We are not aware of any natural examples of zircon or quartz inclusions in pure almandine garnets that could be used to test the EoS of almandine. However, garnets with over 50% almandine component are quite common in metamorphic terranes (e.g. Angiboust et al. 2012; Gilio et al. 2022). To interpret the measured inclusion pressures in these garnets as entrapment conditions the effects of garnet composition must be taken into account. One way to do this is to assume that the elastic properties in garnet solid solutions lie between those of the corresponding end-members, and to estimate the entrapment pressure $P^{\mathrm{mix}}_{\mathrm{trap}}$ at any given T as the average of the P^{i}_{trap} of each end-member component, weighted by its molar fraction X, thus:

$$P^{\mathrm{mix}}_{\mathrm{trap}} = X^{\mathrm{alm}} \bullet P^{\mathrm{alm}}_{\mathrm{trap}} + X^{\mathrm{grs}} \bullet P^{\mathrm{grs}}_{\mathrm{trap}} + X^{\mathrm{prp}} \bullet P^{\mathrm{prp}}_{\mathrm{trap}} + X^{\mathrm{sps}} \bullet P^{\mathrm{sps}}_{\mathrm{trap}} \quad (7)$$

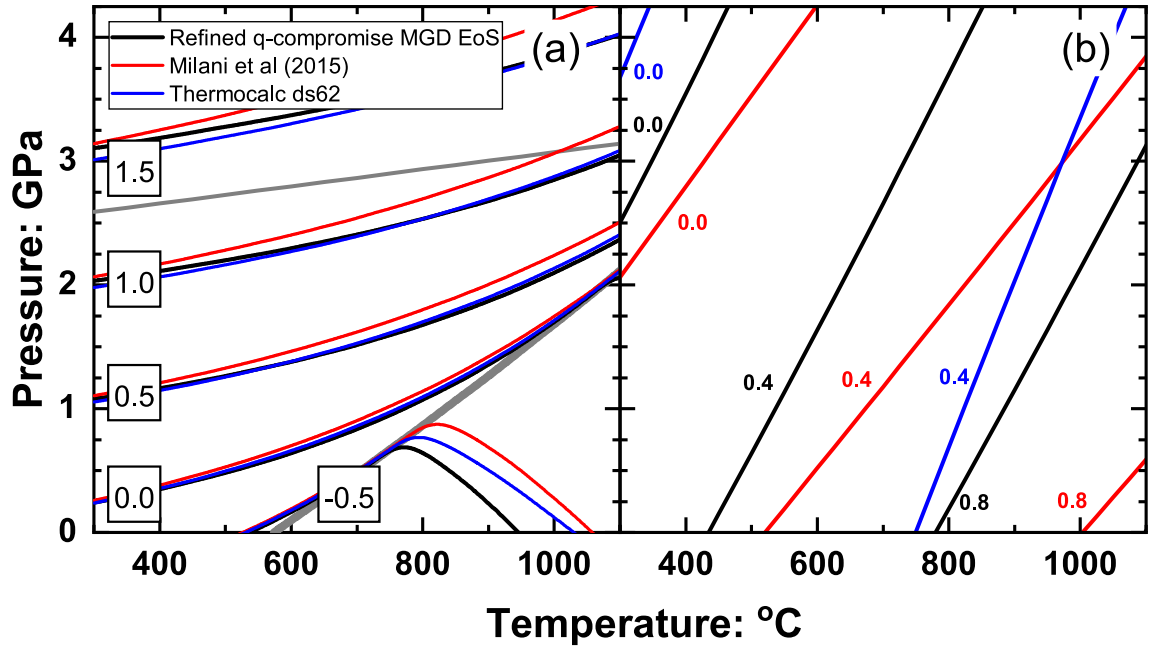

Fig. 17 **a** Entrapment isomekes of quartz (Angel et al. 2017a) with almandine for different EoS. The two grey lines are the phase boundaries for α-quartz = coesite (Bose and Ganguly 1995) and $\alpha = \beta$ quartz. **b** Isomekes of zircon (Ehlers et al. 2022) with different almandine EoS. Numbers in boxes in (**a**) and coloured numbers in (**b**) are the inclusion pressures in GPa that would be measured at room conditions for inclusions trapped on the isomekes

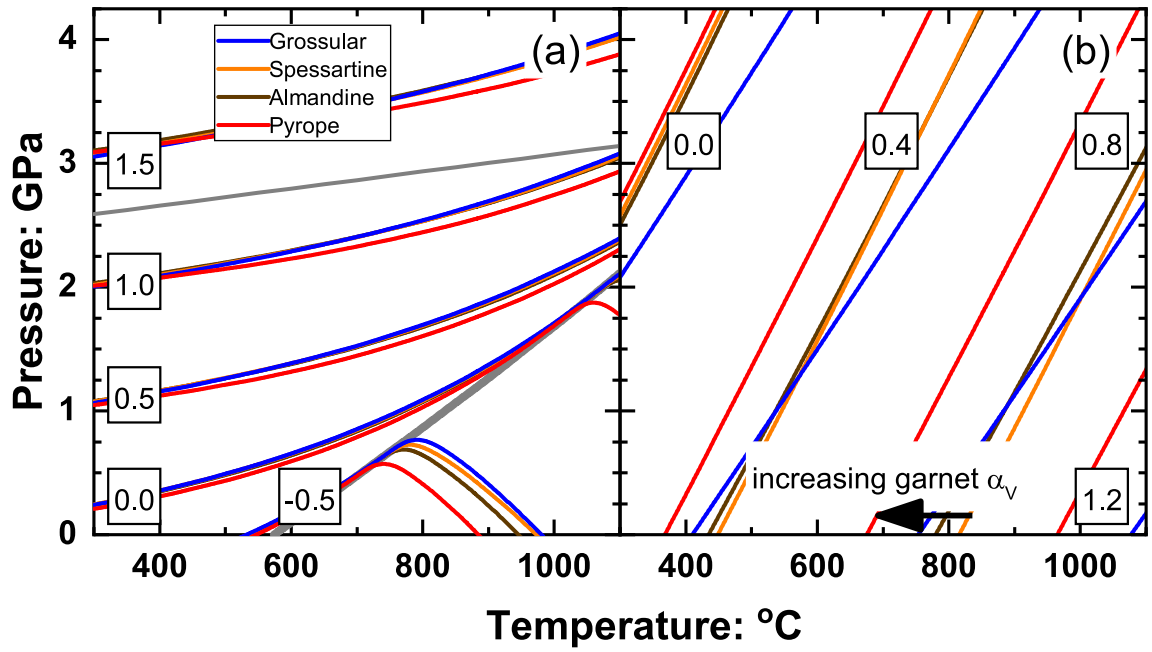

Fig. 18 Entrapment isomekes of the q-compromise MGD EoS of garnets (Table 1) with **a** quartz (Angel et al. 2017a) and **b** zircon (Ehlers et al. 2022). Numbers in boxes are the inclusion pressures in GPa that would be measured at room conditions for inclusions trapped on the isomekes. The two grey lines in **a** are the phase boundaries for α-quartz = coesite (Bose and Ganguly 1995) and $\alpha = \beta$ quartz

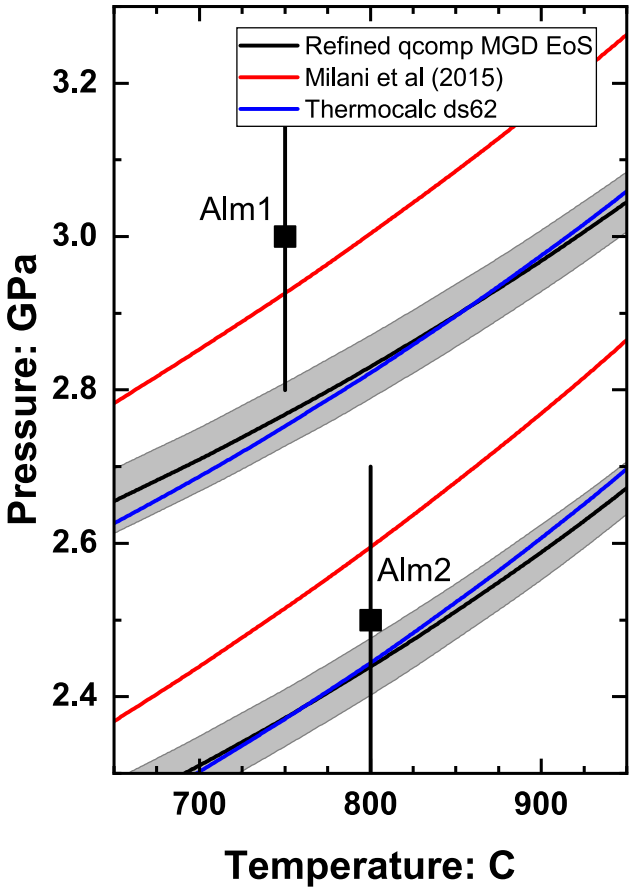

Fig. 19 Isomekes calculated with different EoS from the average residual pressures of quartz inclusions in almandine synthesised in two piston cylinder experiments by Bonazzi et al. (2019). Symbols indicate the conditions of synthesis. The band for *q*-compromise MGD EoS indicates the uncertainties in the calculations from the uncertainties in the EoS parameters; similar uncertainties accompany the other two EoS

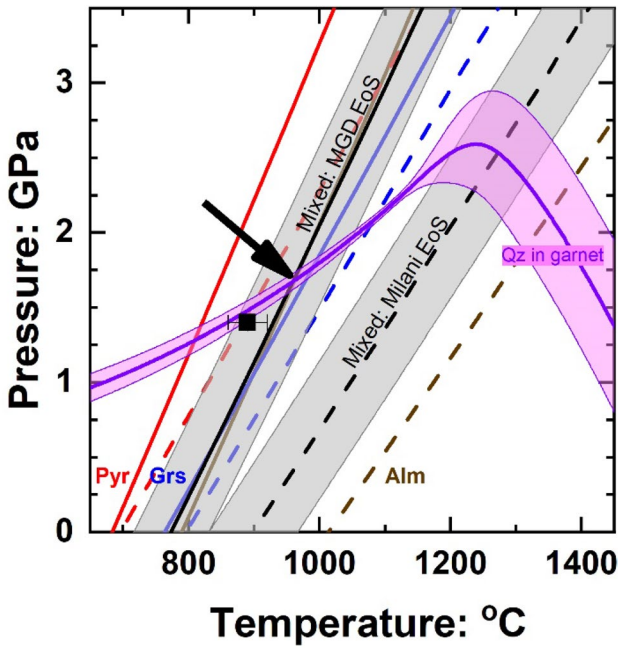

Fig. 20 Isomekes of zircon in end-member garnets calculated with the *q*-compromise MGD EoS (solid lines) and Milani et al. (2015, 2017) EoS (dashed lines) calculated for the average inclusion pressure of 0.84 GPa of zircon inclusions in the rims of the garnets of sample FJ1704 from the Fjørtoft locality in the Western Gneiss Region of Norway (Gilio et al. 2022). The weighted isomeke of zircon from the Milani et al. (2015, 2017) EoS (dashed black line) intersects the isomeke of coeval quartz inclusions (purple line) above 1200 °C, whereas the new *q*-compromise MGD EoS yields entrapment conditions (arrowed) in agreement with independent estimates (symbol) from Gilio et al. (2022). Estimated uncertainties in some isomekes are indicated by shaded bands

Provided that these four garnet end-members represent the greatest part of the true composition, it is unlikely that the small differences of the more uncertain EoS of minor garnet components such as uvarovite or hydrogarnet will significantly change the result, provided that the molar fractions used in Eq. (7) are renormalised to sum to unity.

Figure 20 shows entrapment isomekes of zircon in almandine, grossular and pyrope calculated using the *q*-compromise MGD (full lines) and Milani EoS (dashed lines) for zircon inclusions in the rims of the garnets of sample FJ1704 from the Fjørtoft locality in the Western Gneiss Region of Norway (Gilio et al. 2022). The uncertainty in temperature for these isomekes is ± 50 °C. The corresponding black lines in Fig. 20 are the isomekes calculated with Eq. (7) for the measured garnet composition of $Alm_{0.54}Grs_{0.40}Prp_{0.06}$. Also shown is the entrapment isomeke for the quartz inclusions in the same growth zone of the garnet which are believed to have been trapped at the same time, and thus conditions, as the zircon. Because the isomeke of zircon with almandine from Milani et al. (2015) lies at much higher temperatures than for pyrope or grossular, the average isomeke crosses the quartz-in-garnet isomeke at 1275 ± 75 °C and 2.5 ± 0.5 GPa. These conditions are geologically unreasonable as they approach the melting point of almandine (1250 °C at ambient pressure) and far exceed the temperatures indicated by Zr in rutile thermometry and by the petrology of adjacent units (symbol in Fig. 20). Because the isomekes of zircon with the new *q*-compromise EoS of almandine lie at significantly lower temperatures than those from the Milani et al. (2015) EoS (Figs. 17, 20) the average isomeke produced via Eq. (7) for these zircon inclusions crosses the quartz-in-garnet isomeke at 950 ± 75 °C and 1.7 ± 0.3 GPa, which overlap with PT conditions obtained with other methods and in other structurally adjacent lithologies (Gilio et al. 2022). This suggests that the new EoS for almandine is more accurate than that of Milani et al. (2015).

Unfortunately, spessartine-rich garnet is rare in metamorphic rocks. Most garnets from eclogites and granulites have less than 5% spessartine content although garnets in

metasedimentary rocks have Mn contents that can correspond to as much as 30–50% spessartine component in garnets from (U-)HP oceanic metasediments such as the Lago di Cignana Unit (e.g. Schrojenstein Lantman et al. 2021). However, the calculated isomekes of α-quartz in spessartine (Fig. 18) are within 0.1 GPa of those of almandine and grossular, generally less than the uncertainty in inclusion pressures determined from Raman strain measurements (Gilio et al. 2021). So, although calculated entrapment pressures of quartz inclusions in these garnets are geologically reasonable (Girani 2021; Schrojenstein Lantman et al. 2021) they are not severe tests of the validity of the spessartine EoS. Similarly, the closeness of the isomekes of zircon in almandine to those of spessartine and grossular means that zircon inclusions in natural garnets are also unlikely to provide a test of the almandine EoS.

Conclusions

We have shown that the mutually consistent volume and elasticity data available for the common end-member garnets are consistent within their uncertainties with thermal pressures calculated from experimental C_P values converted to C_V, with the additional assumptions that γ/V is constant and $\left(\partial C_V/\partial P\right)_T = 0$. This confirms that the existing data for these garnets are consistent with the concept of q-compromise EoS in which the sum of the phonon energies (and hence the C_V) does not change significantly with pressure at constant T (equivalent to $q=0$) and that the ratio γ/V is constant (equivalent to $q=1$). The true value of q therefore cannot be significantly greater than 1; indeed, for garnets for which there are sufficient data (pyrope and grossular) to allow independent refinement of q, the refined values (Table 2) are approximately 0.8(2). The use of the q-compromise assumption allows free independent refinement of all the other parameters of the MGD EoS for the garnets discussed here. These MGD EoS provide identical volume and elastic properties at P and T to the Cp-EoS that use the experimental heat capacity data as a basis for calculating the thermal pressure. This is because, although the C_V and thus C_P of a MGD EoS are not correct (Fig. 1), the C_V integral over temperature is quite close to the true integral from room temperature to high temperature and thus provides the correct thermal pressures (e.g. Stixrude and Lithgow-Bertelloni 2005).

Of the major components of metamorphic garnets, there are many datasets for pyrope and grossular and this allows the inconsistent datasets to be easily identified and excluded with the help of Cp-EoS, and the EoS parameters can be determined with small uncertainties (Tables 1, 2). The *PVT* EoS and elastic properties of pyrope and grossular are therefore well-determined. The room-temperature compression curves of almandine and spessartine are also well-constrained, but there is considerable uncertainty associated with their thermal behaviour due to either a lack of data, or inconsistency between datasets. One issue is that while the thermal expansion data of Skinner (1956) for pyrope, grossular and almandine are in error, his data for spessartine (Fig. 12) are not inconsistent with the heat capacity data. The biggest contribution to improving the reliability of these EoS would therefore be new determinations of their thermal expansion at both low and high temperatures and the variation of the bulk modulus with temperature.

There are no obvious trends of the room-temperature values of the thermal expansion coefficients (Table 1) and there is no 'inverse relationship' (Hazen and Finger 1982) between compressibility and thermal expansion coefficient. Thus, pyrope is stiffer than grossular, but its thermal expansion coefficient is also larger at room temperature. Thermal expansion depends on the thermal pressure which in turn is dependent upon the phonon density of states, or vibrational properties of the minerals. These in turn are dependent on not only the bond distances (which control the molar volumes) but also on the bond strengths. For garnets a major factor in determining volumes and bulk modulus is the strength of the bonding in the octahedral site (e.g. Bosenick and Geiger 1997; Woodland et al. 1999; Zhang et al. 1999). Therefore the phonon density of states varies in a complex way between garnets (e.g. Chopelas 2006) so the lack of simple systematics of elastic properties with molar volume is to be expected and is not just a consequence of uncertainties in parameters for some of the garnets.

Despite the lack of systematic trends in the individual parameter values of this set of EoS, we have demonstrated that there are systematic trends in the positions of their isomekes both with quartz and with zircon (Fig. 18). Given that the EoS of pyrope and grossular are well-constrained by the elasticity and volume data, this observation alone is an argument for the reasonableness of the proposed EoS for spessartine and almandine. The biggest change in isomeke positions from previous widely used EoS, and hence inferred geological entrapment pressures and temperatures, is for almandine for which inferred entrapment temperatures of zircon are lowered by ca. 300 °C (Fig. 17) to geologically reasonable conditions (Fig. 20). With this change, measurements of natural inclusions in garnets of intermediate compositions indicate that the entrapment conditions can be reasonably estimated by taking the mean of the entrapment pressures calculated for the end-member components, weighted by their molar abundance in the garnet (Fig. 20).

Supplementary Information The online version contains supplementary material available at https://doi.org/10.1007/s00410-022-01918-5.

Acknowledgements This project was funded from the European Research Council under the European Union's Horizon 2020 research and innovation program grant agreement 714936 TRUE DEPTHS to MA. MLM is supported by an Alexander von Humboldt research fellowship. We thank Herbert Kroll, Charles Geiger, Alix Ehlers and Nancy Ross for discussions and advice on various aspects of this work, and an anonymous reviewer whose comments greatly helped us clarify the description of our analysis methods.

References

Alvaro M, Mazzucchelli ML, Angel RJ, Murri M, Campomenosi N, Scambelluri M, Nestola F, Korsakov AV, Tomilenko AA, Marone F, Morana M (2020) Fossil subduction recorded by quartz from the coesite stability field. Geology 48:24–28. https://doi.org/10.1130/G46617.1

Angel RJ (2000) Equations of state. In: Hazen RM, Downs RT (eds) High-pressure and high-temperature crystal chemistry. Reviews in mineralogy and geochemistry, vol 41. MSA, Wasington, pp 35–60

Angel RJ, Allan DR, Miletich R, Finger LW (1997) The use of quartz as an internal pressure standard in high-pressure crystallography. J Appl Crystallogr 30:461–466

Angel RJ, Gonzalez-Platas J, Alvaro M (2014) EosFit7c and a Fortran module (library) for equation of state calculations. Z Kristallogr 229:405–419

Angel RJ, Alvaro M, Miletich R, Nestola F (2017a) A simple and generalised P-T-V EoS for continuous phase transitions, implemented in EosFit and applied to quartz. Contrib Miner Petrol 172:29. https://doi.org/10.1007/s00410-017-1349-x

Angel RJ, Mazzucchelli ML, Alvaro M, Nestola F (2017b) EosFit-Pinc: a simple GUI for host-inclusion elastic thermobarometry. Am Miner 102:1957–1960. https://doi.org/10.2138/am-2017-6190

Angel RJ, Alvaro M, Nestola F (2018) 40 years of mineral elasticity: a critical review and a new parameterisation of equations of state for mantle olivines and diamond inclusions. Phys Chem Miner 45:95–113

Angel RJ, Murri M, Mihailova B, Alvaro M (2019) Stress, strain and Raman shifts. Z Kristallogr 234:129–140. https://doi.org/10.1515/zkri-2018-2112

Angel RJ, Alvaro M, Schmid-Beurmann P, Kroll H (2020) Commentary on 'constraints on the equations of state of stiff anisotropic minerals: rutile, and the implications for rutile elastic barometry.' Mineral Mag 84:339–347. https://doi.org/10.1180/mgm.2020.14

Angiboust S, Langdon R, Agard P, Waters D, Chopin C (2012) Eclogitization of the Monviso ophiolite (W. Alps) and implications on subduction dynamics. J Metamorph Geol 30:37–61. https://doi.org/10.1111/j.1525-1314.2011.00951.x

Arimoto T, Gréaux S, Irifune T, Zhou C, Higo Y (2015) Sound velocities of $Fe_3Al_2Si_3O_{12}$ almandine up to 19 GPa and 1700 K. Phys Earth Planet Inter 246:1–8. https://doi.org/10.1016/j.pepi.2015.06.004

Armbruster T, Geiger CA, Lager GA (1992) Single-crystal X-ray structure study of synthetic pyrope almandine garnets at 100 and 293 K. Am Miner 77:512–521

Bass JD (1989) Elasticity of grossular and spessartite garnets by Brillouin spectrsocopy. J Geophys Res 94:7621–7628

Bonazzi M, Tumiati S, Thomas J, Angel RJ, Alvaro M (2019) Assessment of the reliability of elastic geobarometry with quartz inclusions. Lithos 350–351:105201. https://doi.org/10.1016/j.lithos.2019.105201

Bose K, Ganguly J (1995) Quartz-coesite transition revisited: reversed experimental determination at 500–1200°C and retrieved thermochemical properties. Am Miner 80:231–238

Bosenick A, Geiger C (1997) Powder X ray diffraction study of synthetic pyrope-grossular garnets between 20 and 295 K. J Geophys Res B 102:22649–22657

Bosenick A, Geiger CA, Cemic L (1996) Heat capacity measurements of synthetic pyrope-grossular garnets between 320 and 1000 K by differential scanning calorimetry. Geochim Cosmochim Acta 60:3251–3227

Chai M, Brown JM (1996) Effects of static non-hydrostatic stress on the R lines of ruby single crystals. Geophys Res Lett 23:3539–3542

Chantel J, Manthilake GM, Frost DJ, Beyer C, Boffa-Ballaran T, Jing Z, Wang Y (2016) Elastic wave velocities in polycrystalline $Mg_3Al_2Si_3O_{12}$-pyrope garnet to 24 GPa and 1300 K. Am Miner 101:991–997. https://doi.org/10.2138/am-2016-5335

Chen G, Cooke JA, Gwanmesia GD, Liebermann RC (1999) Elastic wave velocities of $Mg_3Al_2Si_3O_{12}$-pyrope garnet to 10 GPa. Am Miner 84:384–388

Chopelas A (2006) Modeling the thermodynamic parameters of six endmember garnets at ambient and high pressures from vibrational data. Phys Chem Miner 33:363–376. https://doi.org/10.1007/s00269-006-0065-2

Conrad PG, Zha C-S, Mao HK, Hemley RJ (1999) The high-pressure, single-crystal elasticity of pyrope, grossular, and andradite. Am Miner 84:374–383

Dachs E, Geiger CA (2006) Heat capacities and entropies of mixing of pyrope-grossular ($Mg_3Al_2Si_3O_{12}$-$Ca_3Al_2Si_3O_{12}$) garnet solid solutions: a low-temperature calorimetric and a thermodynamic investigation. Am Miner 91:894–906. https://doi.org/10.2138/am.2006.2005

Dachs E, Geiger CA, Withers AC, Essene EJ (2009) A calorimetric investigation of spessartine: vibrational and magnetic heat capacity. Geochim Cosmochim Acta 73:3393–3409. https://doi.org/10.1016/j.gca.2009.03.011

Dachs E, Geiger CA, Benisek A (2012a) Almandine: lattice and non-lattice heat capacity behavior and standard thermodynamic properties. Am Miner 97:1771–1782. https://doi.org/10.2138/am.2012.4163

Dachs E, Geiger CA, Benisek A, Grevel K-D (2012b) Grossular: a crystal-chemical, calorimetric, and thermodynamic study. Am Miner 97:1299–1313. https://doi.org/10.2138/am.2012.4047

Diella V, Sani A, Levy D, Pavese A (2004) High-pressure synchrotron X-ray diffraction study of spessartine and uvarovite: a comparison between different equation of state models. Am Miner 89:371–376

Du W, Clark SM, Walker D (2015) Thermo-compression of pyrope-grossular garnet solid solutions: non-linear compositional dependence. Am Miner 100:215–222. https://doi.org/10.2138/am-2015-4752

Ehlers AM, Zaffiro G, Angel RJ, Boffa-Ballaran T, Carpenter MA, Alvaro M, Ross NL (2022) Thermoelastic properties of zircon: implications for geothermobarometry. Am Miner 107:74–81. https://doi.org/10.2138/am-2021-7731

Fan D, Xu J, Ma M, Wei S, Zhang B, Liu J, Xie H (2015) P-V-T equation of state of $Ca_3Cr_2Si_3O_{12}$ uvarovite garnet by using a diamond-anvil cell and in-situ synchrotron X-ray diffraction. Am Miner 100:588–597

Geiger CA, Dachs E (2018) Recent developments and the future of low-T calorimetric investigations in the Earth sciences: consequences for thermodynamic calculations and databases. J Metamorph Geol 36:283–295. https://doi.org/10.1111/jmg.12291

Gilio M, Angel RJ, Alvaro M (2021) Elastic geobarometry: how to work with residual inclusion strains and pressures. Am Miner 106:1530–1533. https://doi.org/10.2138/am-2021-7928

Gilio M, Scambelluri M, Angel RJ, Alvaro M (2022) The contribution of elastic geobarometry to the debate on HP versus UHP metamorphism. J Metamorph Geol 40:229–242. https://doi.org/10.1111/jmg.12625

Girani A (2021) Elastic geobarometry applied to the ultra-high pressure Lago di Cignana unit, Western Alps. University of Pavia, Italy

Gonzalez-Platas J, Alvaro M, Nestola F, Angel RJ (2016) EosFit7-GUI: a new GUI tool for equation of state calculations, analyses, and teaching. J Appl Crystallogr 49:1377–1382. https://doi.org/10.1107/S1600576716008050

Greaux S, Kono Y, Nishiyama N, Kunimoto T, Wada K, Irifune T (2011) P-V–T equation of state of $Ca_3Al_2Si_3O_{12}$ grossular garnet. Phys Chem Miner 38:85–94. https://doi.org/10.1007/s00269-010-0384-1

Gréaux S, Yamada A (2014) P-V–T equation of state of $Mn_3Al_2Si_3O_{12}$ spessartine garnet. Phys Chem Miner 41:141–149. https://doi.org/10.1007/s00269-013-0632-2

Gréaux S, Yamada A (2019) Density variations of Cr-rich garnets in the upper mantle inferred from the elasticity of uvarovite garnet. CR Geosci 351:95–103. https://doi.org/10.1016/j.crte.2018.09.012

Gwanmesia GD, Zhang JZ, Darling K, Kung J, Li BS, Wang LP, Neuville D, Liebermann RC (2006) Elasticity of polycrystalline pyrope ($Mg_3Al_2Si_3O_{12}$) to 9 GPa and 1000 °C. Phys Earth Planet Inter 155:179–190. https://doi.org/10.1016/j.pepi.2005.10.008

Gwanmesia GD, Jackson I, Liebermann RC (2007) In search of the mixed derivative $\partial 2M\partial P\partial T$ (M = G, K): joint analysis of ultrasonic data for polycrystalline pyrope from gas- and solid-medium apparatus. Phys Chem Miner 34:85–93. https://doi.org/10.1007/s00269-006-0130-x

Gwanmesia GD, Wang L, Heady A, Liebermann RC (2014) Elasticity and sound velocities of polycrystalline grossular garnet ($Ca_3Al_2Si_3O_{12}$) at simultaneous high pressures and high temperatures. Phys Earth Planet Inter 228:80–87. https://doi.org/10.1016/j.pepi.2013.09.010

Hartwig J, Galkin V (2021) Heat capacity, thermal expansion, and elastic parameters of pyrope. J Therm Anal Calorim 144:71–79. https://doi.org/10.1007/s10973-020-09396-2

Hazen RM, Finger LW (1982) Comparative crystal chemistry. John Wiley and Sons, New York

Hellfrich G, Connolly JAD (2009) Physical contradictions and remedies using simple polythermal equations of state. Am Miner 94:1616–1619

Holland TJB, Powell R (2011) An improved and extended internally consistent thermodynamic dataset for phases of petrological interest, involving a new equation of state for solids. J Metamorph Geol 29:333–383. https://doi.org/10.1111/j.1525-1314.2010.00923.x

Isaak D, Anderson OL, Oda H (1992) High-temperature thermal expansion and elasticity of calcium-rich garnets. Phys Chem Miner 19:106–120

Kieffer SW (1979) Thermodynamics and lattice vibrations of minerals: 1. Mineral heat capacities and their relationships to simple lattice vibrational models. Rev Geophys Space Phys 17:1–19

Kono Y, Gréaux S, Higo Y, Ohfuji H, Irifune T (2010) Pressure and temperature dependences of elastic properties of grossular garnet up to 17 GPa and 1650 K. J Earth Sci 21:782–791

Kroll H, Kirfel A, Heinemann R, Barbier B (2012) Volume thermal expansion and related thermophysical parameters in the Mg, Fe olivine solid-solution series. Eur J Mineral 24:935–956

Kroll H, Schmid-Beurmann P, Sell A, Buescher J, Dohr R, Kirfel A (2019) Thermal expansion and thermal pressure in Co and Ni olivines: a comparison with Mn and Fe olivines. Eur J Mineral 31:313–324. https://doi.org/10.1127/ejm/2019/0031-2805

Leger JM, Redon AM, Chateau C (1990) Compressions of synthetic pyrope, spessartine and uvarovite garnets up to 25 GPa. Phys Chem Miner 17:161–167

Mazzucchelli ML, Angel RJ, Alvaro M (2021) EntraPT: an online application for elastic geothermobarometry. Am Miner 106:829–836. https://doi.org/10.2138/am-2021-7693CCBYNCND

Milani S, Nestola F, Alvaro M, Pasqual D, Mazzucchelli ML, Domeneghetti MC, Geiger C (2015) Diamond–garnet geobarometry: the role of garnet compressibility and expansivity. Lithos 227:140–147

Milani S, Angel RJ, Scandolo L, Mazzucchelli ML, Boffa-Ballaran T, Klemme S, Domeneghetti MC, Miletich R, Scheidl KS, Derzsi M, Tokar K, Prencipe M, Alvaro M, Nestola F (2017) Thermo-elastic behaviour of grossular garnets at high pressures and temperatures. Am Miner 102:851–859. https://doi.org/10.2138/am-2017-5855

Morganti S, Mazzucchelli M, Alvaro M, Reali A (2020) A numerical application of the Eshelby theory for geobarometry of non-ideal host-inclusion systems. Meccanica 55:751–764

Newton RC, Wood BJ (1980) Volume behaviour of silicate solid solutions. Am Miner 65:733–745

Orear J (1982) Least squares when both variables have uncertainties. Am J Phys 50:912–916

Rodehorst U, Carpenter MA, Boffa-Ballaran T, Geiger CA (2004) Local structural heterogeneity, mixing behaviour and saturation effects in the grossular–spessartine solid solution. Phys Chem Miner 31:387–404. https://doi.org/10.1007/s00269-004-0410-2

Ross NL (1992) Latttice vibration and mineral stability. In: Price GD, Ross NL (eds) The stability of minerals. The Mineralogical Society Series, vol 3. Springer, Dordrecht, pp 132–171

Salje E (1995) Chemical mixing and structural phase transitions: the plateau effect and oscillatory zoning near surfaces and interfaces. Eur J Mineral 7:791–806

Scheidl K, Kurnosov A, Trots DM, Boffa-Ballaran T, Angel RJ, Miletich R (2016) Extending the single-crystal quartz pressure gauge to hydrostatic pressures of 19 GPa. J Appl Crystallogr 49:2129–2137. https://doi.org/10.1107/S1600576716015351

Schrojenstein Lantman HW, Scambelluri M, Gilio M, Wallis D, Alvaro M (2021) Extensive fluid–rock interaction and pressure solution in a UHP fluid pathway recorded by garnetite, Lago di Cignana, Western Alps. J Metamorph Geol 39:501–518. https://doi.org/10.1111/jmg.12585

Sinogeikin SV, Bass JD (2000) Single-crystal elasticity of pyrope and MgO to 20 GPa by Brillouin scattering in the diamond cell. Phys Earth Planet Inter 120:43–62

Sinogeikin SV, Bass JD (2002) Elasticity of pyrope and majorite-pyrope solid solutions to high temperatures. Earth Planet Sci Lett 203:549–555

Skinner BJ (1956) Physical properties of end members of the garnet group. Am Miner 41:428–436

Stixrude L, Lithgow-Bertelloni C (2005) Thermodynamics of mantle minerals – I. Physical properties. Geophys J Int 162:610–632

Thiéblot L, Roux J, Richet R (1998) High-temperature thermal expansion and decomposition of garnets. Eur J Mineral 10:7–15

Woodland AB, Angel RJ, Koch M, Kunz M, Miletich R (1999) Equations of state for $Fe^{2+}{}_3Fe^{3+}{}_2Si_3O_{12}$ "skiagite" garnet and Fe_2SiO_4-Fe_3O_4 spinel solid solutions. J Geophys Res Solid Earth 104:20049–20058

Zhang L, Ahsbahs H, Kutoglu A (1998) Hydrostatic compression and crystal structure of pyrope to 33 GPa. Phys Chem Miner 25:301–307

Zhang L, Ahsbahs H, Kutoglu A, Geiger CA (1999) Single-crystal hydrostatic compression of synthetic pyrope, almandine, spessartine, grossular and andradite garnets at high pressures. Phys Chem Miner 27:52–58

Zhong X, Moulas E, Tajčmanová L (2018) Tiny timekeepers witnessing high-rate exhumation processes. Sci Rep 8:2234. https://doi.org/10.1038/s41598-018-20291-7

Zhong X, Moulas E, Tajčmanová L (2020) Post-entrapment modification of residual inclusion pressure and its implications for Raman elastic thermobarometry. Solid Earth 11:223–240. https://doi.org/10.5194/se-11-223-2020

Zou Y, Greaux S, Irifune T, Whitaker ML, Shinmei T, Higo Y (2012a) Thermal equation of state of $Mg_3Al_2Si_3O_{12}$ pyrope garnet up to 19 GPa and 1700 K. Phys Chem Miner 39:589–598. https://doi.org/10.1007/s00269-012-0514-z

Zou Y, Irifune T, Gréaux S, Whitaker ML, Shinmei T, Ohfuji H, Negishi R, Higo Y (2012b) Elasticity and sound velocities of polycrystalline $Mg_3Al_2(SiO_4)_3$ garnet up to 20GPa and 1700K. J Appl Phys 112:014910